Inorganic Chemistry

pubs.acs.org/IC Article

Bis(phosphine)hydridorhodacarborane Derivatives of 1,1′-Bis(*ortho*-carborane) and Their Catalysis of Alkene Isomerization and the Hydrosilylation of Acetophenone

Antony P.Y. Chan, John A. Parkinson, Georgina M. Rosair, and Alan J. Welch*

Cite This: https://dx.doi.org/10.1021/acs.inorgchem.9b03351 Read Online

ABSTRACT: Deprotonation of [7-(1′-*closo*-1′,2′-$C_2B_{10}H_{11}$)-*nido*-7,8-$C_2B_9H_{11}$]$^-$ and reaction with [Rh(PPh$_3$)$_3$Cl] results in isomerization of the metalated cage and the formation of [8-(1′-*closo*-1′,2′-$C_2B_{10}H_{11}$)-2-H-2,2-(PPh$_3$)$_2$-*closo*-2,1,8-RhC$_2$B$_9$H$_{10}$] (**1**). Similarly, deprotonation/metalation of [8′-(7-*nido*-7,8-$C_2B_9H_{11}$)-2′-(*p*-cymene)-*closo*-2′,1′,8′-RuC$_2$B$_9$H$_{10}$]$^-$ and [8′-(7-*nido*-7,8-$C_2B_9H_{11}$)-2′-Cp*-*closo*-2′,1′,8′-CoC$_2$B$_9$H$_{10}$]$^-$ affords [8-{8′-2′-(*p*-cymene)-*closo*-2′,1′,8′-RuC$_2$B$_9$H$_{10}$}-2-H-2,2-(PPh$_3$)$_2$-*closo*-2,1,8-RhC$_2$B$_9$H$_{10}$] (**2**) and [8-(8′-2′-Cp*-*closo*-2′,1′,8′-CoC$_2$B$_9$H$_{10}$)-2-H-2,2-(PPh$_3$)$_2$-*closo*-2,1,8-RhC$_2$B$_9$H$_{10}$] (**3**), respectively, as diastereoisomeric mixtures. The performances of compounds **1**−**3** as catalysts in the isomerization of 1-hexene and in the hydrosilylation of acetophenone are compared with those of the known single-cage species [3-H-3,3-(PPh$_3$)$_2$-*closo*-3,1,2-RhC$_2$B$_9$H$_{11}$] (**I**) and [2-H-2,2-(PPh$_3$)$_2$-*closo*-2,1,12-RhC$_2$B$_9$H$_{11}$] (**V**), the last two compounds also being the subjects of ^{103}Rh NMR spectroscopic studies, the first such investigations of rhodacarboranes. In alkene isomerization all the 2,1,8- or 2,1,12-RhC$_2$B$_9$ species (**1**−**3**, **V**) outperform the 3,1,2-RhC$_2$B$_9$ compound **I**, while for hydrosilylation the single-cage compounds **I** and **V** are better catalysts than the double-cage species **1**−**3**.

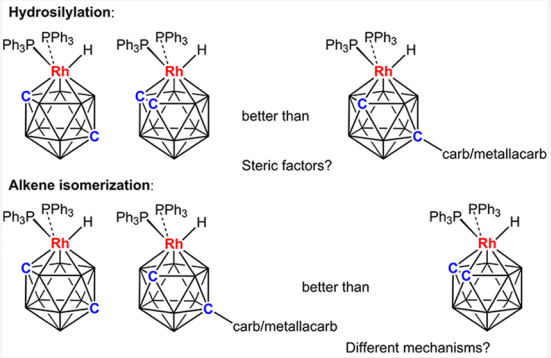

INTRODUCTION

Both the importance and the extent of metallacarboranes as catalysts or catalyst precursors have recently been summarized by Grimes.[1] In the vast majority of such cases the metallacarborane is MC$_2$B$_9$, existing either as a closed icosahedron (Figure 1, left) or in an *exonido* form (Figure 1, right) in which the metal fragment is appended to the *nido* carborane by external links, frequently B−H-M bridges.

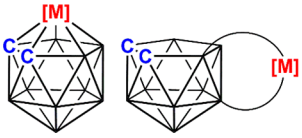

Figure 1. (left) Generic MC$_2$B$_9$ metallacarborane in the *closo*-icosahedral form. (right) *Exonido* metallacarborane. No specific point of attachment of the metal fragment to the cage is implied.

The archetypal metallacarborane catalyst precursor is [3-H-3,3-(PPh$_3$)$_2$-*closo*-3,1,2-RhC$_2$B$_9$H$_{11}$] (**I**, Figure 2), which was found to catalyze a number of reactions including alkene isomerization and hydrogenation.[2] For these reactions it was concluded from the results of kinetic and deuterium labeling studies that the *closo* form **I** (Rh^{III}) is in equilibrium with an *exonido* tautomer **II** (Rh^{I}). It is believed that this, in turn, is in equilibrium with an exo Rh^{III} species **III**, the result of oxidative

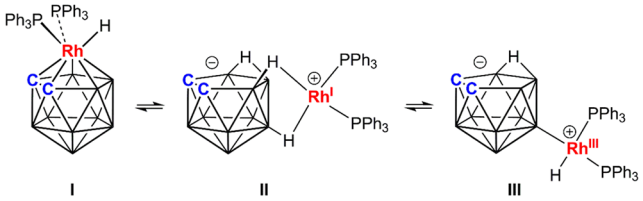

Figure 2. Suggested tautomerism between *closo* rhodacarborane **I**, *exonido* intermediate **II**, and immediate catalyst precursor **III**.

insertion of the metal into a B−H bond, and that dissociation of one PPh$_3$ from **III** affords the active catalyst.[3] Although neither **III** nor an analog have ever been isolated it has been possible to stabilize and fully characterize (including a crystallographic study) an analog of the *exonido* species **II** with a 1′,2′-CH$_2$C$_6$H$_4$CH$_2$− bridge on the cage C atoms and a mixed PPh$_3$/PCy$_3$ ligand set on Rh.[4]

There have been relatively few studies in which the catalytic activity of **I** is tuned by modification. The 2,1,7-RhC$_2$B$_9$ (**IV**)

Received: November 18, 2019

and 2,1,12-RhC_2B_9 (**V**) isomeric analogs of **I** (Figure 3) have been studied, as have compounds in which various substituents

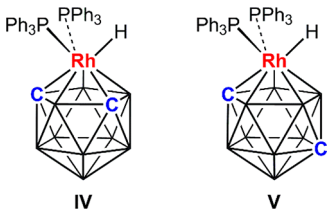

Figure 3. 2,1,7-RhC_2B_9 (**IV**) and 2,1,12-RhC_2B_9 (**V**) isomers of **I**.

are attached to one or both cage C atoms,[2b,4] and/or the exopolyhedral ligand set is altered.[2b,4] Of relevance to the present work is the observation that one such derivative, [1-^{n}Bu-3-H-3,3-$(PPh_3)_2$-*closo*-3,1,2-$RhC_2B_9H_{10}$], isomerizes to the less-sterically crowded isomer [8-^{n}Bu-2-H-2,2-$(PPh_3)_2$-*closo*-2,1,8-$RhC_2B_9H_{10}$] under mild conditions.[2b] Other notable modifications to the parent catalyst precursor **I** include partial *B*-fluorination[5] and its incorporation into phosphazene-based polymers.[6]

Recent years have witnessed significant interest in the synthesis and applications of derivatives of bis(carboranes).[7] The simplest bis(carborane), [1-(1′-*closo*-1′,2′-$C_2B_{10}H_{11}$)-*closo*-1,2-$C_2B_{10}H_{11}$] (**VI**, Figure 4), colloquially known as

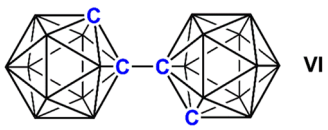

Figure 4. 1,1′-Bis(*ortho*-carborane).

1,1′-bis(*ortho*-carborane), offers a versatile scaffold for derivatization making it an attractive candidate for use in catalysis. Recently, we have reported the metalation of 1,1′-bis(*ortho*-carborane) to afford both metallacarborane−carborane[8] and metallacarborane−metallacarborane species, the latter of which we have prepared in both homometalated[9] and heterometalated forms.[10] In seeking to expand this chemistry we have now targeted bis(carborane) analogs of **I** as potential new precatalysts. Herein we describe the synthesis, characterization, and catalytic properties of species in which the additional carborane cage not only functions as a large, electron-withdrawing substituent to **I** but also provides a scaffold which can be metalated. The catalytic properties of these new species are compared against those of **I** and **V**, and for completeness we also report full spectroscopic and structural characterization of **V** and the first ^{103}Rh NMR studies of rhodacarboranes, the single-cage species **I** and **V**.

■ EXPERIMENTAL SECTION

Synthesis and Catalysis. Experiments were performed under dry, oxygen-free N_2 using standard Schlenk techniques, although subsequent manipulations were sometimes performed in the open laboratory. Solvents were freshly distilled under nitrogen from the appropriate drying agent [THF and 40−60 petroleum ether (petrol); sodium wire: CH_2Cl_2 (DCM); calcium hydride] and were degassed (3 × freeze−pump−thaw cycles) before use. Deuterated solvents for NMR spectroscopy ($CDCl_3$, CD_2Cl_2) were stored over 4 Å molecular sieves. Preparative TLC employed 20 × 20 cm^2 Kieselgel F_{254} glass plates and column chromatography used 60 Å silica as the stationary phase. Elemental analyses were conducted using an Exeter CE-440 elemental analyzer. NMR spectra at 400.1 MHz (^{1}H), 128.4 MHz (^{11}B) and 162.0 MHz (^{31}P) were recorded on a Bruker AVANCEIII-400 NMR spectrometer at Heriot-Watt University using samples solubilized in CD_2Cl_2 at room temperature unless otherwise stated. ^{103}Rh NMR spectra were recorded at the University of Strathclyde NMR Facility using a combination of either direct observation ^{103}Rh-{^{1}H}-INEPT or indirect 2D [^{1}H, ^{103}Rh] HMQC NMR data acquisitions on a 14.1 T Bruker AVANCE II$^+$-600 NMR spectrometer operating at 600.130 MHz for ^{1}H observation and 18.964108 MHz as the ^{103}Rh zero reference resonance frequency. A Bruker BBO-z-ATM probe-head suitable for automated tuning and matching (ATM) to the resonant frequency of tungsten (^{183}W = 24.966 MHz) was adapted for manual tuning and matching to a resonant frequency suitable for working with ^{103}Rh. All NMR spectra were recorded at a probe temperature of 298 K. Full experimental details of the ^{103}Rh NMR study are described in the Supporting Information (SI). Electron ionization mass spectrometry (EIMS) and electrospray ionization mass spectrometry (ESIMS) were carried out using a Bruker MicroTOF Focus II mass spectrometer and a Thermo MAT900XP-Trap mass spectrometer, respectively, at the University of Edinburgh. The starting materials [3-H-3,3-$(PPh_3)_2$-*closo*-3,1,2-$RhC_2B_9H_{11}$] (**I**),[2b] [2-H-2,2-$(PPh_3)_2$-*closo*-2,1,12-$RhC_2B_9H_{11}$] (**V**),[11] 1,1′-bis(*ortho*-carborane) (**VI**),[12] [$Rh(PPh_3)_3Cl$],[13] [$HNMe_3$][7-(1′-*closo*-1′,2′-$C_2B_{10}H_{11}$)-*nido*-7,8-$C_2B_9H_{11}$] ([$HNMe_3$]**VII**),[8] [$HNMe_3$]-[8′-(7-*nido*-7,8-$C_2B_9H_{11}$)-2′-(*p*-cymene)-*closo*-2′,1′,8′-$RuC_2B_9H_{10}$] ([$HNMe_3$]**VIII**)[10,14] and [$HNMe_3$][8′-(7-*nido*-7,8-$C_2B_9H_{11}$)-2′-Cp*-*closo*-2′,1′,8′-$CoC_2B_9H_{10}$] ([$HNMe_3$]**IX**)[10,14] were prepared by literature methods or slight variations thereof. All other reagents were supplied commercially.

*[8-(1′-closo-1′,2′-$C_2B_{10}H_{11}$)-2-H-2,2-$(PPh_3)_2$-closo-2,1,8-$RhC_2B_9H_{10}$] (**1**).* ^{n}BuLi (0.41 mL of a 1.6 M solution in hexanes, 0.656 mmol) was added dropwise to a cooled (0 °C) solution of [$HNMe_3$]**VII** (0.100 g, 0.298 mmol) in THF (15 mL), and the products were stirred for 1 h at room temperature. The pale yellow solution was frozen at −196 °C, and [$Rh(PPh_3)_3Cl$] (0.276 g, 0.298 mmol) was added and the reaction mixture allowed to thaw and stir overnight. The mixture was filtered through silica, the solvents were removed *in vacuo* and the residue purified by column chromatography using a DCM/petrol eluent, 1:1, to afford a yellow band. R_f 0.44. Yield 0.142 g, 0.157 mmol, 53%. $C_{40}H_{52}B_{19}P_2Rh$ requires: C 53.2, H 5.80. Found: C 54.1, H 5.99%. ^{1}H NMR δ 7.67−7.13 (m, 30H, C_6H_5), 1.95 (br s, 1H, C2′*H*), 1.84 (br s, 1H, C1*H*), −8.70 (ddd, 1H, Rh*H*, J_{RhH} = 26.9 Hz, J_{PH} = 26.9, 15.4 Hz). ^{11}B{^{1}H} NMR δ −0.8 to −13.1 multiple overlapping resonances with maxima at −0.8, −3.3, −4.4, −6.1, −10.5, −13.1 (total integral 16B), −17.4 to −19.1 multiple overlapping resonances with maxima at −17.4, −19.1 (total integral 3B). ^{31}P{^{1}H} NMR δ 35.82 (dd, 1P, J_{RhP} = 114.9 Hz, J_{PP} = 27.7 Hz), 32.93 (dd, 1P, J_{RhP} = 107.0 Hz, J_{PP} = 27.7 Hz). Neither EIMS nor ESIMS afforded useful results. Note that in this and following metalation reactions, the isolated yields are reasonable in the context of bis(carborane) metalations. Multiple mobile bands are frequently observed upon purification by chromatography but these are typically isolated in trace amounts prohibiting further analysis. Additionally, the nonmobile components removed from silica with acetonitrile and studied by ^{11}B{^{1}H} NMR spectroscopy typically reveal resonances around δ −30 to −40 ppm, characteristic of *nido*-7,8-C_2B_9 fragments. We therefore ascribe the relatively low yields to poor conversion and/or multiple products as opposed to decomposition.

*α-[8-{8′-2′-(p-cymene)-closo-2′,1′,8′-$RuC_2B_9H_{10}$}-2-H-2,2-$(PPh_3)_2$-closo-2,1,8-$RhC_2B_9H_{10}$] (**2α**) and β-[8-{8′-2′-(p-cymene)-closo-2′,1′,8′-$RuC_2B_9H_{10}$}-2-H-2,2-$(PPh_3)_2$-closo-2,1,8-$RhC_2B_9H_{10}$] (**2β**).* ^{n}BuLi (0.12 mL of a 1.6 M solution in hexanes, 0.192 mmol) was added dropwise to a cooled (0 °C) solution of [$HNMe_3$]**VIII** (0.050 g, 0.089 mmol) in THF (15 mL). Following warming to room temperature, the yellow solution was frozen at −196 °C and [$Rh(PPh_3)_3Cl$] (0.083 g, 0.090 mmol) was added. Once thawed, the reaction mixture was heated to reflux overnight. Following cooling and filtration through silica, solvents were removed *in vacuo* and the residue purified by preparative TLC using a DCM/petrol eluent in a 1:1 ratio to afford two major colorless bands.

https://dx.doi.org/10.1021/acs.inorgchem.9b03351
Inorg. Chem. XXXX, XXX, XXX−XXX

*α-[8-{8′-2′-(p-cymene)-closo-2′,1′,8′-RuC$_2$B$_9$H$_{10}$}-2-H-2,2-(PPh$_3$)$_2$-closo-2,1,8-RhC$_2$B$_9$H$_{10}$] (**2α**).* R_f 0.28. Yield 0.021 g, 0.019 mmol, 21%. $C_{50}H_{65}B_{18}P_2RhRu$ requires: C 53.3, H 5.82. Found: C 54.5, H 6.08%. ^{1}H NMR δ 7.43−7.09 (m, 30H, C$_6$H$_5$), 5.74−5.63 [m, 4H, CH$_3$C$_6$H$_4$CH(CH$_3$)$_2$], 2.70 [app sept, 1H, CH$_3$C$_6$H$_4$CH(CH$_3$)$_2$], 2.45 (br s, 1H, C1′H), 2.17 [s, 3H, CH$_3$C$_6$H$_4$CH(CH$_3$)$_2$], 1.31 (br s, 1H, C1H), 1.23 [d, 3H, CH$_3$C$_6$H$_4$CH(CH$_3$)$_2$], 1.21 [d, 3H, CH$_3$C$_6$H$_4$CH(CH$_3$)$_2$], −8.56 (ddd, 1H, RhH, J_{RhH} = 29.8 Hz, J_{PH} = 23.7, 15.4 Hz). ^{11}B{^{1}H} NMR δ 0.2 to −8.6 multiple overlapping resonances with maxima at 0.2, −1.7, −5.2, −8.6 (total integral 12B), −15.7 to −21.0 multiple overlapping resonances with maxima at −15.7, −16.5, −21.0 (total integral 6B). ^{31}P{^{1}H} NMR δ 36.95 (dd, 1P, J_{RhP} = 114.9 Hz, J_{PP} = 26.8 Hz), 32.65 (dd, 1P, J_{RhP} = 109.0 Hz, J_{PP} = 26.8 Hz). EIMS: envelope centered on *m/z* 603 (M$^+$-2 × PPh$_3$).

*β-[8-{8′-2′-(p-cymene)-closo-2′,1′,8′-RuC$_2$B$_9$H$_{10}$}-2-H-2,2-(PPh$_3$)$_2$-closo-2,1,8-RhC$_2$B$_9$H$_{10}$] (**2β**). R_f 0.35.* Yield 0.033 g, 0.029 mmol, 33%. $C_{50}H_{65}B_{18}P_2RhRu$ requires: C 53.3, H 5.82. Found: C 53.4, H 5.86%. ^{1}H NMR δ 7.42−7.09 (m, 30H, C$_6$H$_5$), 5.79−5.66 [m, 4H, CH$_3$C$_6$H$_4$CH(CH$_3$)$_2$], 2.71 [app sept, 1H, CH$_3$C$_6$H$_4$CH(CH$_3$)$_2$], 2.45 (br s, 1H, C1′H), 2.20 [s, 3H, CH$_3$C$_6$H$_4$CH(CH$_3$)$_2$], 1.33 (br s, 1H, C1H), 1.24 [d, 3H, CH$_3$C$_6$H$_4$CH(CH$_3$)$_2$], 1.22 [d, 3H, CH$_3$C$_6$H$_4$CH(CH$_3$)$_2$], −8.57 (ddd, 1H, RhH, J_{RhH} = 30.1 Hz, J_{PH} = 23.7, 14.7 Hz). ^{11}B{^{1}H} NMR δ 0.0 to −8.5 multiple overlapping resonances with maxima at 0.0, −5.1, −8.5 (total integral 12B), −15.8 to −21.1 multiple overlapping resonances with maxima at −15.8, −16.6, −21.1 (total integral 6B). ^{31}P{^{1}H} NMR δ 36.99 (dd, 1P, J_{RhP} = 113.0 Hz, J_{PP} = 25.8 Hz), 32.62 (dd, 1P, J_{RhP} = 109.0 Hz, J_{PP} = 25.8 Hz). EIMS: envelope centered on *m/z* 603 (M$^+$-2 × PPh$_3$).

α-[8-(8′-2′-Cp-closo-2′,1′,8′-CoC$_2$B$_9$H$_{10}$)-2-H-2,2-(PPh$_3$)$_2$-closo-2,1,8-RhC$_2$B$_9$H$_{10}$] (**3α**) and β-[8-(8′-2′-Cp*-closo-2′,1′,8′-CoC$_2$B$_9$H$_{10}$)-2-H-2,2-(PPh$_3$)$_2$-closo-2,1,8-RhC$_2$B$_9$H$_{10}$] (**3β**).* ^{n}BuLi (0.13 mL of a 1.6 M solution in hexanes, 0.208 mmol) was added dropwise to a cooled (0 °C) solution of [HNMe$_3$]**IX** (0.050 g, 0.097 mmol) in THF (15 mL). Following warming to room temperature, the dark yellow solution was frozen at −196 °C and [Rh(PPh$_3$)$_3$Cl] (0.090 g, 0.097 mmol) was added and the reaction mixture allowed to thaw to room temperature and stir overnight. Following filtration through silica, solvents were removed *in vacuo* and the residue purified by preparative TLC using a DCM/petrol eluent in a 1:1 ratio to afford two major pale yellow bands.

α-[8-(8′-2′-Cp-closo-2′,1′,8′-CoC$_2$B$_9$H$_{10}$)-2-H-2,2-(PPh$_3$)$_2$-closo-2,1,8-RhC$_2$B$_9$H$_{10}$] (**3α**). R_f* 0.36. Yield 0.017 g, 0.016 mmol, 16%. $C_{50}H_{66}B_{18}CoP_2Rh$ requires: C 55.3, H 6.13. Found: C 55.8, H 6.08%. ^{1}H NMR δ 7.42−7.09 (m, 30H, C$_6$H$_5$), 1.74 [s, 15H, C$_5$(CH$_3$)$_5$], 1.65 (br s, 1H, C1′H), 1.40 (br s, 1H, C1H), −8.57 (ddd, 1H, RhH, J_{RhH} = 30.3 Hz, J_{PH} = 24.2, 15.6 Hz). ^{11}B{^{1}H} NMR δ 0.9 to −8.5 multiple overlapping resonances with maxima at 0.9, −6.0, −8.5 (total integral 12B), −14.7 to −22.0 multiple overlapping resonances with maxima at −14.7, −15.5, −19.6, −22.0 (total integral 6B). ^{31}P{^{1}H} NMR δ 37.35 (dd, 1P, J_{RhP} = 113.0 Hz, J_{PP} = 22.8 Hz), 32.51 (dd, 1P, J_{RhP} = 109.0 Hz, J_{PP} = 22.8 Hz). ESIMS: envelope centered on *m/z* 822 (M$^+$-PPh$_3$).

β-[8-(8′-2′-Cp-closo-2′,1′,8′-CoC$_2$B$_9$H$_{10}$)-2-H-2,2-(PPh$_3$)$_2$-closo-2,1,8-RhC$_2$B$_9$H$_{10}$] (**3β**). R_f* 0.41. Yield: 0.019 g, 0.018 mmol, 18%. $C_{50}H_{66}B_{18}CoP_2Rh$ requires: C 55.3, H 6.13. Found: C 56.2, H 6.11%. ^{1}H NMR δ: 7.42−7.09 (m, 30H, C$_6$H$_5$), 1.75 [s, 15H, C$_5$(CH$_3$)$_5$], 1.66 (br s, 1H, C1′H), 1.38 (br s, 1H, C1H), −8.58 (ddd, 1H, RhH, J_{RhH} = 28.9 Hz, J_{PH} = 23.0, 14.2 Hz). ^{11}B{^{1}H} NMR δ: 0.8 to −8.4 multiple overlapping resonances with maxima at 0.8, −6.7, −8.4 (total integral 12B) and −14.9 to −21.9 multiple overlapping resonances with maxima at −14.9, −15.5, −19.0, −21.9 (total integral 6B). ^{31}P{^{1}H} NMR δ: 37.18 (dd, 1P, J_{RhP} = 113.0 Hz, J_{PP} = 26.8 Hz), 32.54 (dd, 1P, J_{RhP} = 109.0 Hz, J_{PP} = 26.8 Hz). ESIMS: envelope centered on *m/z* 822 (M$^+$−PPh$_3$).

*Further Spectroscopic Characterization of **I** and **V**. [3-H-3,3-(PPh$_3$)$_2$-closo-3,1,2-RhC$_2$B$_9$H$_{10}$] (**I**).* ^{103}Rh{^{1}H} NMR δ: −972.93 (t, J_{RhP} = 125.7 Hz).

*[2-H-2,2-(PPh$_3$)$_2$-closo-2,1,12-RhC$_2$B$_9$H$_{10}$] (**V**).* ^{1}H NMR δ: 7.68−6.94 (m, 30H, C$_6$H$_5$), 2.34 (br s, 1H, C12H), 1.49 (br s, 1H, C1H), −8.79 (dt, 1H, RhH, J_{RhH} = 27.4 Hz, J_{PH} = 14.9 Hz). ^{11}B{^{1}H} NMR δ: −1.4 (1B), −6.5 (2B), −9.2 (2B), −19.7 (4B). ^{31}P{^{1}H} NMR δ: 36.12 (d, 2P, J_{RhP} = 111.0 Hz). ^{103}Rh{^{1}H} NMR δ: −922.48 (t, J_{RhP} = 111.0 Hz). For ^{103}Rh chemical shift referencing, see a later description of the ^{103}Rh NMR study and the accompanying Supporting Information.

General Procedure for Alkene Isomerization. A J. Young NMR tube was flushed with N$_2$ and charged with 1-hexene (188 μL, 1.503 mmol) and mesitylene (internal standard, 104 μL, 0.748 mmol). A CDCl$_3$ (1 mL) solution of the catalyst precursor (0.003 mmol) was added, and the progress of the reaction monitored by ^{1}H NMR spectroscopy. Further details are available in the SI.

General Procedure for Ketone Hydrosilylation. Acetophenone (37 μL, 0.317 mmol), diphenylsilane (74 μL, 0.399 mmol), and mesitylene (internal standard, 22 μL, 0.158 mmol) were combined in a J. Young NMR tube previously flushed with N$_2$. A CDCl$_3$ (1 mL) solution of the catalyst precursor (0.0016 mmol) was added, and the reagents were heated to 55 °C; the progress of the reaction was monitored by ^{1}H NMR spectroscopy. Further details are available in the SI.

Crystallography. Single crystals of **1**·0.5CH$_2$Cl$_2$, **2α**·2CH$_2$Cl$_2$, **3α**·2.5CH$_2$Cl$_2$, and **V** were grown by diffusion of a DCM solution of the appropriate compound and petrol at −20 °C. Crystals of **2β**·1.5CH$_2$Cl$_2$ were obtained by vapor diffusion of a DCM solution and petrol at −20 °C, while single crystals of **3β**·2.5CH$_2$Cl$_2$ were afforded by slow evaporation of a DCM solution at room temperature. Diffraction data were obtained from **3α**·2.5CH$_2$Cl$_2$ and **3β**·2.5CH$_2$Cl$_2$ on a Bruker X8 APEXII diffractometer operating with Mo *Kα* radiation. Data from **1**·0.5CH$_2$Cl$_2$ were obtained on a Rigaku AFC12 diffractometer using Mo *Kα* radiation. Data from **2α**·2CH$_2$Cl$_2$ and **2β**·1.5CH$_2$Cl$_2$ were obtained on a Rigaku 007HF diffractometer using Cu *Kα* radiation. Data from **V** were obtained on a Bruker D8 Venture diffractometer equipped with Mo *Kα* radiation. All diffraction data were collected at 100 K except for that of **V** (150 K). Structures were solved using OLEX2[15] by direct methods using the SHELXS[16] or SHELXT[17] program and were refined by full-matrix least-squares using SHELXL.[18] All crystals except **V** contain DCM of solvation, all of which was impossible to model satisfactorily. Crystals of **1** contain 0.5DCM per molecule of **1**, but this could not be modeled. In **2α** there are 2DCM per molecule of **2α**, only one of which could be modeled. Crystals of **2β** have 1.5DCM per molecule, but this was not possible to model. **3α** and **3β** are isomorphous, with both having 2.5DCM per molecule of **3**, but two of these could not be modeled while the remaining 0.5DCM could be. In all cases the intensity contribution of the badly disordered solvent was removed using the BYPASS procedure[19] implemented in OLEX2. In **1**·0.5CH$_2$Cl$_2$, **2α**·2CH$_2$Cl$_2$, **2β**·1.5CH$_2$Cl$_2$, and **V** application of the vertex-centroid distance (VCD) and boron−hydrogen distance (BHD) methods[20] allowed cage C atoms bearing only H substituents to be clearly distinguished from B atoms. Compounds **3α**·2.5CH$_2$Cl$_2$ and **3β**·2.5CH$_2$Cl$_2$ have two crystallographically independent molecules present in the asymmetric fraction of the unit cell, thus eight metallacarborane cages in total. In these cages refinement of only some of the cage H atoms was possible, and so the BHD method had limited applicability. Nevertheless, in all eight cages C atoms were identified unambiguously by the VCD approach. In all the compounds studied the electron density corresponding to the Rh-bound hydride ligand was located, but only in the case of **1**·0.5CH$_2$Cl$_2$ and **V** did positional refinement of the hydride lead to a chemically sensible model. For **2α**·2CH$_2$Cl$_2$, **2β**·1.5CH$_2$Cl$_2$, **3α**·2.5CH$_2$Cl$_2$, and **3β**·2.5CH$_2$Cl$_2$, the hydride ligands were therefore restrained to Rh−H = 1.58(2) Å and P···H = 2.55(2) Å, these distances being taken from the successful hydride refinement in **1**·0.5CH$_2$Cl$_2$. For **1**·0.5CH$_2$Cl$_2$, **2α**·2CH$_2$Cl$_2$, and **2β**·1.5CH$_2$Cl$_2$, cage H atoms were allowed positional refinement, while for **3α**·2.5CH$_2$Cl$_2$ and **3β**·2.5CH$_2$Cl$_2$, they were set in idealized positions riding on their B or C atom with B−H = 1.12 Å and C$_{cage}$−H = 1.00 Å. All other H atoms were also treated as riding, with C$_{phenyl}$−H = 0.95 Å, C$_{primary}$−H = 0.98 Å, C$_{tertiary}$−H = 1.00 Å, and C$_{arene}$−H = 1.00 Å. H atom displacement parameters were constrained to 1.2 × U_{eq} (bound B or C) except for

https://dx.doi.org/10.1021/acs.inorgchem.9b03351
Inorg. Chem. XXXX, XXX, XXX−XXX

Me H atoms [1.5 × U_{eq} (C_{methyl})] and the hydride (U_H 0.02 Å^2). The SI contains unit cell data and further experimental details.

■ RESULTS AND DISCUSSION

Synthesis and Characterization. Hawthorne's classic approach to inserting a {RhH(PPh_3)$_2$} fragment into a *nido* carborane is to heat a solution of the carborane anion with [Rh(PPh_3)$_3$Cl],[2] and indeed, we have used this method to prepare his single cage species **I** and **V** for comparison of catalytic performance with the new compounds reported herein. However, this protocol does not necessarily work well if the carborane anion has a *closo* carborane substituent, i.e., is singly deboronated 1,1′-bis(*ortho*-carborane). Thus, reaction of [Tl][7-(1′-*closo*-1′,2′-$C_2B_{10}H_{11}$)-*nido*-7,8-$C_2B_9H_{11}$] ([Tl]**VII**) with [Rh(PPh_3)$_3$Cl] yields only the cation-exchanged product [Rh(PPh_3)$_3$][7-(1′-*closo*-1′,2′-$C_2B_{10}H_{11}$)-*nido*-7,8-$C_2B_9H_{11}$],[4] a possible factor being an unfavorable steric clash between the incoming metal fragment and the bulky carborane substituent on the open face.

In an attempt to overcome this unfavorable steric factor with an increased favorable Coulombic one, we have first deprotonated anion **VII** and then attempted metalation. Thus, following treatment of [HNMe$_3$]**VII** with two equivalents of ^{n}BuLi in THF, addition of [Rh(PPh_3)$_3$Cl] afforded the yellow target compound [8-(1′-*closo*-1′,2′-$C_2B_{10}H_{11}$)-2-H-2,2-(PPh_3)$_2$-*closo*-2,1,8-$RhC_2B_9H_{10}$] (**1**) in 53% yield following workup involving column chromatography (Scheme 1).

Scheme 1. Deprotonation and Subsequent Metalation of Anion VII to Afford Compound 1

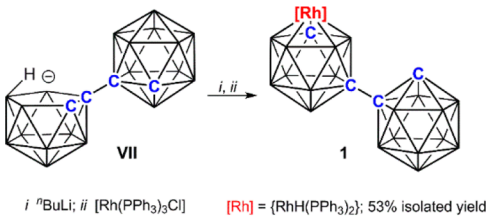

Compound **1** was initially characterized by elemental analysis which was consistent with the molecular formula $C_{40}H_{52}B_{19}P_2Rh$. The ^{1}H NMR spectrum contains a multiplet between δ ca. 7.7 and 7.1 ppm for 30 phenyl protons, two broad integral-1 $C_{cage}H$ resonance (δ ca. 2.0 and 1.8 ppm), and an integral-1 hydride resonance at δ −8.7 ppm appearing as a doublet of doublet of doublets due to splitting by the rhodium atom and two inequivalent phosphorus atoms. It is assumed that the hydride ligand originates from solvent during synthesis or workup. The $C_{cage}H$ resonances are at relatively low frequency compared to those in the related species [8-(1′-*closo*-1′,2′-$C_2B_{10}H_{11}$)-2-(*p*-cymene)-*closo*-2,1,8-$RuC_2B_9H_{10}$] and [8-(1′-*closo*-1′,2′-$C_2B_{10}H_{11}$)-2-Cp*-*closo*-2,1,8-$CoC_2B_9H_{10}$], but this is usually observed in metallacarboranes when {Ru(arene)} or {CoCp/Cp*} fragments are replaced by formally isolobal {RhH(PPh_3)$_2$} fragments (see Table 1); a possible explanation is offered below following discussion of the structure of **1**. By comparison with the metallacarborane−carboranes noted, we tentatively assign the resonance in **1** at δ 1.84 ppm to the $C_{cage}H$ of the rhodacarborane and that at δ 1.95 ppm to the $C_{cage}H$ of the carborane substituent. The ^{11}B{^{1}H} NMR spectrum is largely uninformative due to a number of overlapping resonances, but two regions can be clearly distinguished (δ −0.8 to −13.1 and −17.4 to −19.1 ppm) with relative integrals of 16 and 3 respectively, summing to the anticipated 19 boron atoms. Two equal-integral doublets of doublets are observed in the ^{31}P{^{1}H} NMR spectrum (δ 35.8 and 32.9 ppm), consistent with two unique phosphorus environments as implied by the splitting of the hydride resonance and indicative of an asymmetric RhC_2B_9 cage.

The structure of **1** was confirmed crystallographically, and a perspective view of a single molecule is shown in Figure 5. C_{cage} atoms not involved in the intercage C−C link were identified unambiguously using the VCD and BHD methods,[20] and thus **1** is established as the 2,1,8-RhC_2B_9-1′,2′-C_2B_{10} isomer with rearrangement of the metalated cage having occurred to avoid untenable steric congestion. Compound **1** is thus analogous to [8-(1′-1′,2′-*closo*-$C_2B_{10}H_{11}$)-2-H-2,2-(PEt_3)$_2$-2,1,8-*closo*-$RhC_2B_9H_{10}$], prepared by treatment of [Rh(PPh_3)$_3$][7-(1′-*closo*-1′,2′-$C_2B_{10}H_{11}$)-*nido*-7,8-$C_2B_9H_{11}$] with PEt_3,[4a] and to [8-(1′-1′,2′-*closo*-$C_2B_{10}H_{11}$)-2-H-2,2-(PPh_3)$_2$-2,1,8-*closo*-$IrC_2B_9H_{10}$], prepared by thermolysis of [(COD)Ir(PPh_3)][7-(1′-*closo*-1′,2′-$C_2B_{10}H_{11}$)-*nido*-7,8-$C_2B_9H_{11}$],[25] although neither of these analogs were characterized crystallographically.

In the rhodacarborane cage of **1** the orientation of the {RhH(PPh_3)$_2$} fragment is such that the hydride ligand lies *trans* to C1, an exopolyhedral ligand orientation (ELO) which is fully consistent with the relative structural *trans* effects (STE) of H and PPh_3.[20c] As a direct result of this the Rh2−C1 connectivity is considerably weaker than the Rh−B connectivities and, in spite of the smaller atomic radius of C compared to B, significantly longer, at 2.306(4) Å vs 2.175(4)−2.215(4) Å. We believe that this relatively weak Rh−C bonding results in relatively strong C1−H bonding which is reflected in a low-frequency shift of the C1*H* resonance (δ 1.84 ppm) in the ^{1}H NMR spectrum of **1** as noted above, an argument supported by structural and spectroscopic comparisons between [3-H-3,3-(PPh_3)$_2$-*closo*-3,1,2-$RhC_2B_9H_{11}$] (**I**) and [3-Cl-3,3-(PPh_3)$_2$-*closo*-3,1,2-$RhC_2B_9H_{11}$] (**X**). In the solid-state structure of **I** the strong-STE H ligand lies *trans* to one C_{cage} atom (which makes the longest Rh-cage atom connectivity),[20a] while in solution the time-averaged structure has mirror symmetry and the δ $C_{cage}H$ is 2.24 ppm (CD_2Cl_2).[2a] Two separate crystallographic studies of **X** reveal a molecule in which the weak-STE Cl ligand lies over the C−C connectivity with the Rh−C distances shorter than those of Rh−B,[23] and in CD_2Cl_2 solution the $C_{cage}H$ atoms resonate at δ 3.77 ppm.[23b] Thus, there is established a link between ELO, Rh−cage atom distance, and $C_{cage}H$ chemical shift; a strong-STE ligand lies *trans* to cage C, causing a weak (and long) Rh−C connectivity and a strong C−H bond manifested in a low-frequency ^{1}H NMR chemical shift. The same pattern can be noted in the isoelectronic and isostructural anions [3-X-3,3-(PPh_3)$_2$-*closo*-$RuC_2B_9H_{11}$]$^-$ (X = H, Cl) for which δ $C_{cage}H$ is 1.63 (X = H) and 2.90 (X = Cl) ppm in $(CD_3)_2CO$.[24]

Having established a good protocol for inserting the {RhH(PPh_3)$_2$} fragment into bis(carborane), we have used this approach for [*nido*-7,8-C_2B_9-*closo*-2′,1′,8′-MC_2B_9]$^-$ salts, M = {Ru(*p*-cymene)} and {CoCp*}, as starting points in the synthesis of mixed-metal RhRu and RhCo species. Deprotonation of [HNMe$_3$]**VIII** in THF with ^{n}BuLi followed by addition of [Rh(PPh_3)$_3$Cl] and heating to reflux overnight afforded the rhodacarborane−ruthenacarborane species **2** as a mixture of diastereoisomers, separated by preparative TLC

https://dx.doi.org/10.1021/acs.inorgchem.9b03351
Inorg. Chem. XXXX, XXX, XXX−XXX

Table 1. Cage C*H* Chemical Shifts in 1−3 and Related Species

species	δ(C*H*)/ppm (assignment)	solvent	ref
[3-(*p*-cymene)-*closo*-3,1,2-$RuC_2B_9H_{11}$]	3.70 (C1*H*, C2*H*)	$CDCl_3$	21
[3-Cp*-*closo*-3,1,2-$CoC_2B_9H_{11}$]	2.95 (C1*H*, C2*H*)	$CDCl_3$	22
[3-H-3,3-$(PPh_3)_2$-*closo*-3,1,2-$RhC_2B_9H_{11}$] (**I**)	2.24 (C1*H*, C2*H*)	CD_2Cl_2	2a
[3-Cl-3,3-$(PPh_3)_2$-*closo*-3,1,2-$RhC_2B_9H_{11}$] (**X**)	3.77 (C1*H*, C2*H*)	CD_2Cl_2	23b
[3-H-3,3-$(PPh_3)_2$-*closo*-3,1,2-$RuC_2B_9H_{11}$]$^-$	1.63 (C1*H*, C2*H*)	$(CD_3)_2CO$	24
[3-Cl-3,3-$(PPh_3)_2$-*closo*-3,1,2-$RuC_2B_9H_{11}$]$^-$	2.90 (C1*H*, C2*H*)	$(CD_3)_2CO$	24
[2-H-2,2-$(PPh_3)_2$-*closo*-2,1,12-$RhC_2B_9H_{11}$] (**V**)	2.34 (C12*H*), 1.49 (C1*H*)	CD_2Cl_2	this work
[1-(1′-1′,2′-*closo*-$C_2B_{10}H_{11}$)-3-(*p*-cymene)-3,1,2-*closo*-$RuC_2B_9H_{10}$]	4.03, 3.91 (not assigned)	$CDCl_3$	8a
[1-(1′-1′,2′-*closo*-$C_2B_{10}H_{11}$)-3-Cp*-3,1,2-*closo*-$CoC_2B_9H_{10}$]	4.10 (C2′*H*), 3.37 (C2*H*)	$CDCl_3$	10
[8-(1′-1′,2′-*closo*-$C_2B_{10}H_{11}$)-2-(*p*-cymene)-2,1,8-*closo*-$RuC_2B_9H_{10}$]	3.64 (C2′*H*), 2.63 (C1*H*)	$CDCl_3$	8a
[8-(1′-1′,2′-*closo*-$C_2B_{10}H_{11}$)-2-Cp*-2,1,8-*closo*-$CoC_2B_9H_{10}$]	4.01 (C2′*H*), 2.09 (C1*H*)	CD_3CN[a]	10
[8-(1′-1′,2′-*closo*-$C_2B_{10}H_{11}$)-2-H-2,2-$(PPh_3)_2$-2,1,8-*closo*-$RhC_2B_9H_{10}$] (**1**)	1.95 (C2′*H*), 1.84 (C1*H*)	CD_2Cl_2	this work
[8′-(7-*nido*-7,8-$C_2B_9H_{11}$)-2′-(*p*-cymene)-*closo*-2′,1′,8′-$RuC_2B_9H_{10}$]$^-$ (**VIII**)	2.64 (C1*H*), 1.93 (C8′*H*)	$(CD_3)_2CO$	10
[8′-(7-*nido*-7,8-$C_2B_9H_{11}$)-2′-Cp*-*closo*-2′,1′,8′-$CoC_2B_9H_{10}$] (**IX**)	1.96 (C1*H*), 1.88 (C8′*H*)	$(CD_3)_2CO$	10
α-[8-(1′-3′-Cp-*closo*-3′,1′,2′-$CoC_2B_9H_{10}$)-2-(*p*-cymene)-*closo*-2,1,8-$RuC_2B_9H_{10}$]	4.27 (C2′*H*), 2.63 (C1*H*)	$CDCl_3$	10
β-[8-(1′-3′-Cp-*closo*-3′,1′,2′-$CoC_2B_9H_{10}$)-2-(*p*-cymene)-*closo*-2,1,8-$RuC_2B_9H_{10}$]	4.12 (C2′*H*), 2.63 (C1*H*)	$CDCl_3$	10
[8-{8′-2′-(*p*-cymene)-*closo*-2′,1′,8′-$RuC_2B_9H_{10}$}-2-Cp*-*closo*-2,1,8-$CoC_2B_9H_{10}$] (major)	2.59 (C1′*H*), 1.74 (C1*H*)	$CDCl_3$	10
[8-{8′-2′-(*p*-cymene)-*closo*-2′,1′,8′-$RuC_2B_9H_{10}$}-2-Cp*-*closo*-2,1,8-$CoC_2B_9H_{10}$] (minor)	2.62 (C1′*H*), 1.77 (C1*H*)	$CDCl_3$	10
α-[8-{8′-2-(*p*-cymene)-*closo*-2′,1′,8′-$RuC_2B_9H_{10}$}-2-H-2,2-$(PPh_3)_2$-*closo*-2,1,8-$RhC_2B_9H_{10}$] (**2**α)	2.45 (C1′*H*), 1.31 (C1*H*)	CD_2Cl_2	this work
β-[8-{8′-2-(*p*-cymene)-*closo*-2′,1′,8′-$RuC_2B_9H_{10}$}-2-H-2,2-$(PPh_3)_2$-*closo*-2,1,8-$RhC_2B_9H_{10}$] (**2**β)	2.45 (C1′*H*), 1.33 (C1*H*)	CD_2Cl_2	this work
α-[8-(8′-2-Cp*-*closo*-2′,1′,8′-$CoC_2B_9H_{10}$)-2-H-2,2-$(PPh_3)_2$-*closo*-2,1,8-$RhC_2B_9H_{10}$] (**3**α)	1.65 (C1′*H*), 1.40 (C1*H*)	CD_2Cl_2	this work
β-[8-(8′-2-Cp*-*closo*-2′,1′,8′-$CoC_2B_9H_{10}$)-2-H-2,2-$(PPh_3)_2$-*closo*-2,1,8-$RhC_2B_9H_{10}$] (**3**β)	1.66 (C1′*H*), 1.38 (C1*H*)	CD_2Cl_2	this work

[a] $CHCl_3/CD_3CN$, 1:10

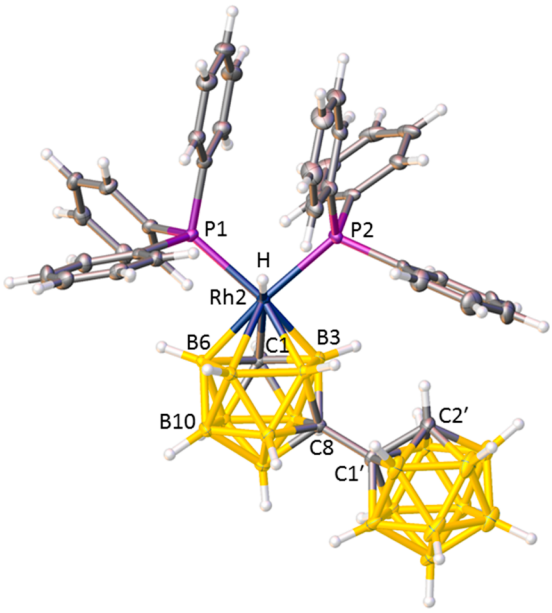

Figure 5. Perspective view of compound **1** with displacement ellipsoids drawn at the 50% probability level except for H atoms. Selected interatomic distances (Å): Rh2−C1 2.306(4), Rh2−B3 2.175(4), Rh2−B7 2.196(4), Rh2−B11 2.215(4), Rh2−B6 2.206(6), Rh2−P1 2.3581(10), Rh2−P2 2.3384(10), Rh2−H 1.58(4), C8−C1′ 1.524(5), C1′−C2′ 1.638(6).

into **2**α and **2**β (Scheme 2). Note that, to facilitate comparisons with **I** and **1**, the rhodacarborane has been labeled as the unprimed cage and the ruthenacarborane as the primed cage, whereas previously we have labeled according to the order the metal fragments were inserted, unprimed first and primed second.[10]

Compounds **2**α and **2**β were isolated as very pale yellow solids in yields of 21% and 33%, respectively, and satisfactory

Scheme 2. Deprotonation and Subsequent Metalation of Anion VIII to Afford Compounds 2α and 2β as a Diastereoisomeric Mixture

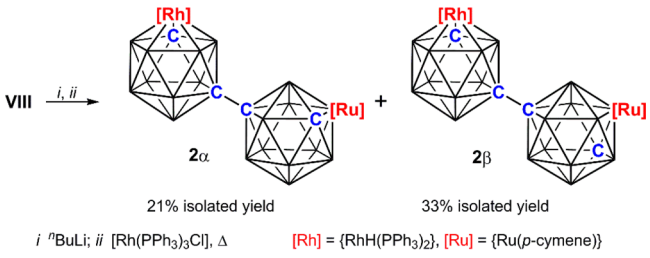

mass spectrometric and microanalytical results were obtained for both. The NMR spectra of **2**α and **2**β are almost identical, as anticipated. The ^{1}H NMR spectra display the expected resonances for the triphenylphosphine and *p*-cymene ligands in the correct integral ratio. $C_{cage}H$ resonances are observed at δ ca. 2.4 and 1.3 ppm and, by comparison with the chemical shift of the $C_{cage}H$ of the ruthenacarborane in [8-(1′-1′,2′-*closo*-$C_2B_{10}H_{11}$)-2-(*p*-cymene)-2,1,8-*closo*-$RuC_2B_9H_{10}$] (δ 2.63 ppm) and two isomers of [8-{8′-2′-(*p*-cymene)-*closo*-2′,1′,8′-$RuC_2B_9H_{10}$}-2-Cp*-*closo*-2,1,8-$CoC_2B_9H_{10}$] (δ 2.59, 2.62 ppm, Table 1), the higher frequency signal is assigned to the already-present ruthenacarborane cage and the lower frequency signal to the new rhodacarborane cage. Additionally, in the spectra of both **2**α and **2**β a resonance is found at δ ca. −8.6 ppm with the same ddd splitting pattern observed for compound **1**. $^{11}B\{^1H\}$ NMR spectroscopy gives little insight into the nature of **2**α and **2**β due to the large number of overlapping resonances. Two regions of signals are observed (from δ ca. 0 to −9 and −16 to −21 ppm) with relative integrals of 12 and 6, summing to the expected 18 B atoms. As was also the case with **1**, two resonances are observed in the $^{31}P\{^1H\}$ NMR spectra of **2**α and **2**β, at δ ca. 37 and 33 ppm, appearing as doublets of

https://dx.doi.org/10.1021/acs.inorgchem.9b03351
Inorg. Chem. XXXX, XXX, XXX−XXX

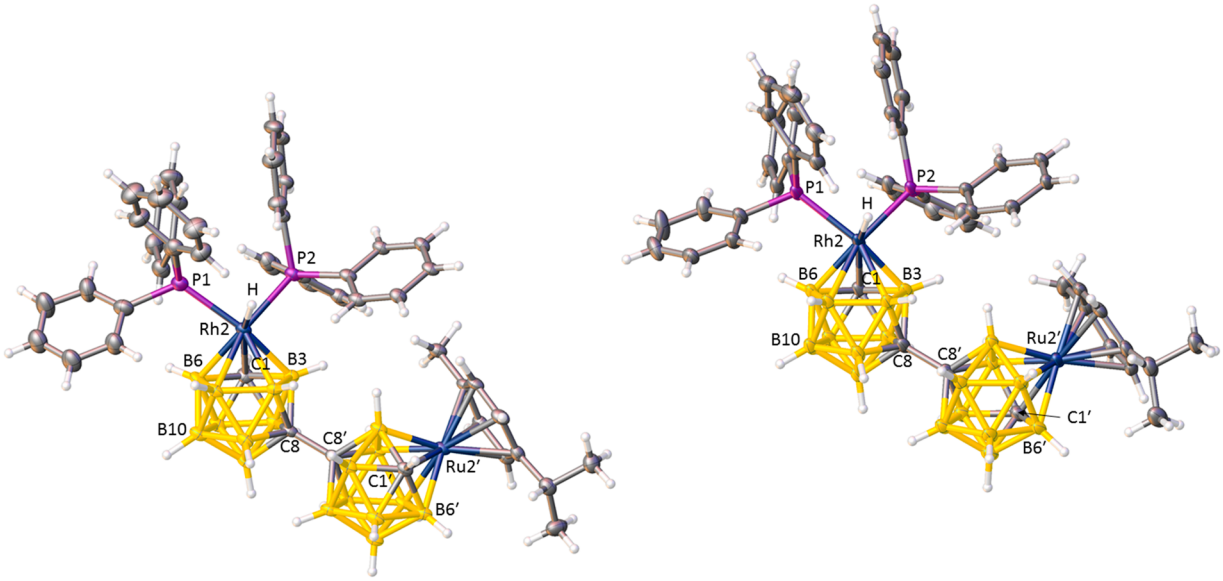

Figure 6. (left) Perspective view of compound **2***α* with displacement ellipsoids as in Figure 5. Selected interatomic distances (Å): Rh2−C1 2.287(5), Rh2−B3 2.184(6), Rh2−B7 2.227(6), Rh2−B11 2.228(5), Rh2−B6 2.222(6), Rh2−P1 2.3747(16), Rh2−P2 2.3479(12), Ru2′−C1′ 2.163(5), Ru2′−B 2.160(6)−2.214(5), C8−C8′ 1.537(7). (right) Perspective view of compound **2***β* with displacement ellipsoids as in Figure 5. Selected interatomic distances (Å): Rh2−C1 2.278(5), Rh2−B3 2.172(5), Rh2−B7 2.230(4), Rh2−B11 2.246(4), Rh2−B6 2.216(5), Rh2−P1 2.3664(10), Rh2−P2 2.3407(9), Ru2′−C1′ 2.177(4), Ru2′−B 2.152(4)−2.214(4), C8−C8′ 1.553(5).

doublets. In anion **VIII**, the precursor to **2***α* and **2***β*, the ruthenacarborane is already in the 2,1,8-RuC_2B_9 isomeric form. The $C_{cage}H$ atoms of the rhodacarborane cages resonate at δ ca. 1.3 ppm, closer to that in the 2,1,8-RhC_2B_9 species **1** (1.84 ppm) than that in the 3,1,2-RhC_2B_9 compound **I** (2.24 ppm). Thus, we postulate that in **2** the rhodacarborane is also in the 2,1,8-RhC_2B_9 form and consequently that **2***α* and **2***β* are a diastereomeric mixture of [8-{8′-2′-(*p*-cymene)-*closo*-2′,1′,8′-$RuC_2B_9H_{10}$}-2-H-2,2-$(PPh_3)_2$-*closo*-2,1,8-$RhC_2B_9H_{10}$].

This was subsequently confirmed crystallographically. Critical to the assignment of the correct isomeric form of the molecule is the identification of the cage C atoms not involved in the intercage bond, and despite the fact that crystals of **2***α* and **2***β* were relatively weakly diffracting, C atom identification was achieved unambiguously by application of the VCD and BHD methods.[20]

The structures of **2***α* and **2***β* are shown in Figure 6. The two molecules are practically superimposable save for the position of C1′ in the ruthenacarborane cage (which distinguishes the two different diastereoisomers) and a slight difference in the orientations of the *p*-cymene ligands. As was the case with **1**, the $\{RhH(PPh_3)_2\}$ fragments are orientated such that the hydride ligands are effectively *trans* to C1, resulting in the Rh−C1 connectivities being the longest of the Rh−cage atom links. In contrast, in the ruthenacarborane cages the *p*-cymene ligand exhibits no preferred ELO and the Ru−C1′ connectivity lies within the range of Ru−B lengths, close to the shortest such connectivity.

Rhodacarborane−cobaltacarborane species were afforded analogously. Deprotonation of $[HNMe_3]$**IX** followed by reaction with $[Rh(PPh_3)_3Cl]$ at room temperature produced [8-(8′-2′-Cp*-*closo*-2′,1′,8′-$CoC_2B_9H_{10}$)-2-H-2,2-$(PPh_3)_2$-*closo*-2,1,8-$RhC_2B_9H_{10}$] (**3**) as a diastereoisomeric mixture. Preparative TLC readily separated the diastereoisomers to afford compounds **3***α* and **3***β* as pale yellow solids in isolated yields of 16% and 18%, respectively (Scheme 3). The

Scheme 3. Deprotonation and Subsequent Metalation of Anion IX to Afford Compounds 3*α* and 3*β* as a Diastereoisomeric Mixture

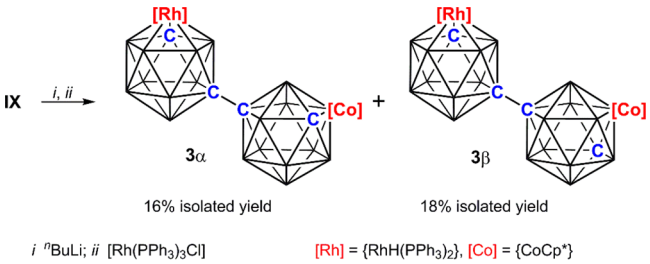

molecular formula $C_{50}H_{66}B_{18}CoP_2Rh$ was established by elemental analysis and mass spectrometry. As was the case with **2**, NMR spectra of **3***α* and **3***β* are very similar. In addition to resonances arising from the 30 phenyl H atoms and the 15 H atoms of Cp* ligand, two $C_{cage}H$ resonances (δ ca. 1.7 and 1.4 ppm) and a hydride resonance (ddd, δ ca. −8.6 ppm) are observed in both the ^1H NMR spectra. With reference to the data in Table 1, we tentatively assign the higher frequency $C_{cage}H$ resonances to the cobaltacarborane cage and the lower frequency one to the new rhodacarborane cage. Similarly to those of compounds **2**, the $^{11}B\{^1H\}$ NMR spectra of **3***α* and **3***β* show two regions of overlapping resonances with relative integrals of 12 and 6, summing to 18 B atoms, and the $^{31}P\{^1H\}$ NMR spectra display two doublet of doublets at δ ca. 37 and 32 ppm. On the basis of the spectral similarities between **2** and **3** we conclude that **3** also has an isomerized 2,1,8-RhC_2B_9-2′,1′,8′-M′C_2B_9 architecture.

This was subsequently confirmed crystallographically. Compounds **3***α* and **3***β* crystallize with 2.5 molecules of DCM per molecule of **3** and are isomorphous, with two independent molecules in the asymmetric fraction of the unit cell. The determinations of **3***α* and **3***β* are relatively imprecise, and not all cage H atoms could be positionally refined,

https://dx.doi.org/10.1021/acs.inorgchem.9b03351
Inorg. Chem. XXXX, XXX, XXX−XXX

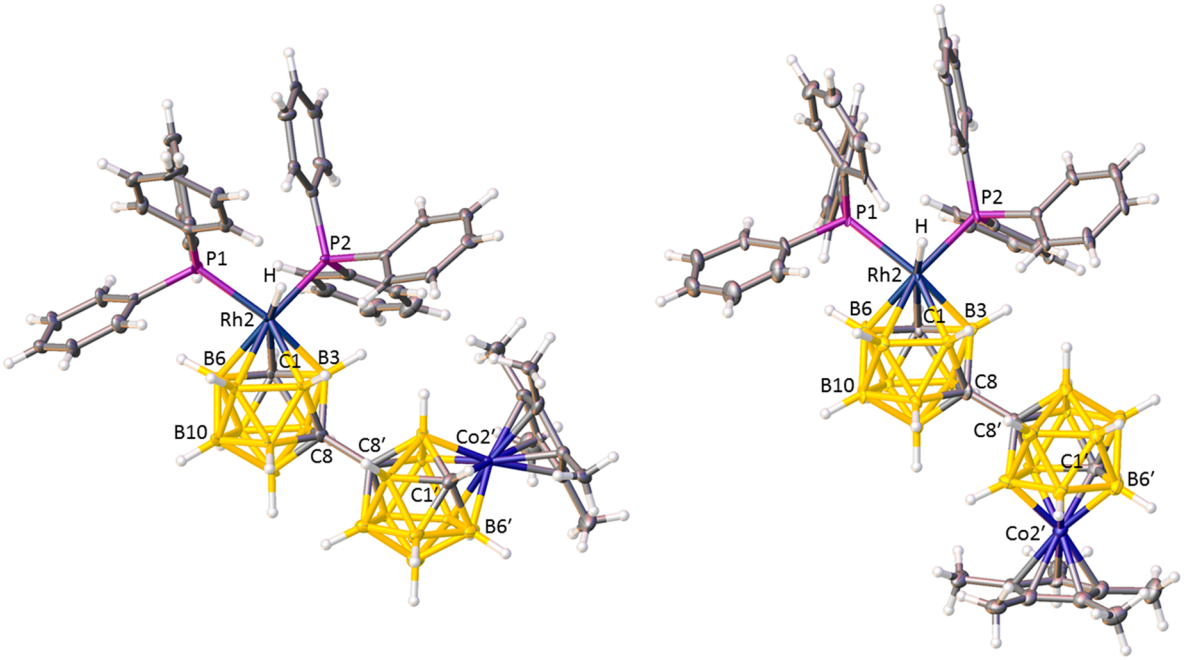

Figure 7. Perspective views of the two crystallographically independent molecules of compound **3***α* with displacement ellipsoids as in Figure 5. Selected interatomic distances and torsion angles (Å, °): (left) Rh2−C1 2.252(13), Rh2−B3 2.203(14), Rh2−B7 2.243(14), Rh2−B11 2.251(14), Rh2−B6 2.247(13), Rh2−P1 2.357(3), Rh2−P2 2.348(3), Co2′−C1′ 2.022(13), Co2′−B 2.041(14)−2.104(14), C8−C8′ 1.538(17), Rh2···C8−C8′···Co2′ −32.2(2). (right) Rh2−C1 2.288(12), Rh2−B3 2.193(14), Rh2−B7 2.214(14), Rh2−B11 2.255(15), Rh2−B6 2.227(15), Rh2−P1 2.363(3), Rh2−P2 2.334(3), Co2′−C1′ 2.024(14), Co2′−B 1.996(14)−2.109(15), C8−C8′ 1.548(18), Rh2···C8−C8′···Co2′ −176.7(5).

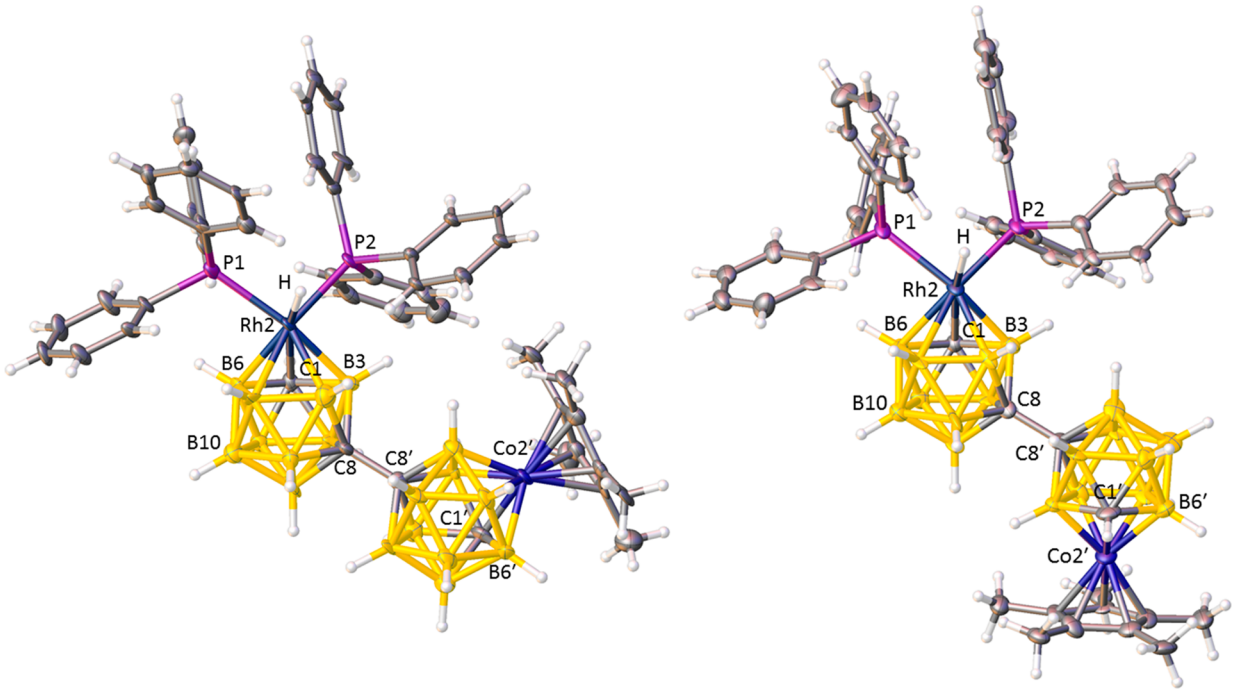

Figure 8. Perspective views of the two crystallographically independent molecules of compound **3***β* with displacement ellipsoids as in Figure 5. Selected interatomic distances and torsion angles (Å, °): (left) Rh2−C1 2.293(12), Rh2−B3 2.218(15), Rh2−B7 2.246(17), Rh2−B11 2.256(16), Rh2−B6 2.193(15), Rh2−P1 2.377(4), Rh2−P2 2.385(4), Co2′−C1′ 2.035(14), Co2′−B 2.021(17)−2.079(17), C8−C8′ 1.571(18), Rh2···C8−C8′···Co2′ −31(3). (right) Rh2−C1 2.276(13), Rh2−B3 2.193(15), Rh2−B7 2.225(16), Rh2−B11 2.306(16), Rh2−B6 2.239(15), Rh2−P1 2.388(4), Rh2−P2 2.366(4), Co2′−C1′ 2.041(14), Co2′−B 2.005(18)−2.099(19), C8−C8′ 1.596(18), Rh2···C8−C8′···Co2′ 178.8(5).

rendering the BHD method unsuitable for cage C identification. Nevertheless in all eight metallacarborane cages application of the VCD method unambiguously identified atoms C1 and C1′, confirming compound **3** as [8-(8′-2′-Cp*-*closo*-2′,1′,8′-$CoC_2B_9H_{10}$)-2-H-2,2-$(PPh_3)_2$-*closo*-2,1,8-$RhC_2B_9H_{10}$]. Figure 7 shows the two independent molecules of **3***α* and Figure 8 those of **3***β*.

https://dx.doi.org/10.1021/acs.inorgchem.9b03351
Inorg. Chem. XXXX, XXX, XXX−XXX

The two independent molecules in each of **3**α and **3**β differ in respect of the torsion about the C8−C8′ bond. One molecule (on the left in Figures 7 and 8) has Rh2···C8−C8′···Co2′ ca. −30° [similar to the Rh2···C8−C8′···Ru2′ angles in **2**α and **2**β, −36.0(7)° and −33.5(6)°, respectively], while in the other molecule (on the right in the figures) the metal atoms are effectively *trans* to one another. Although the structures of **3**α and **3**β are relatively imprecise it is clear that in all cases the orientation of the $\{RhH(PPh_3)_2\}$ fragment is, as expected, that in which the hydride ligand sits *trans* to C1, with the large STE of the hydride resulting in a relatively long Rh−C1 connectivity.

In summary, we have prepared and characterized five new bis(phosphine)hydridorhodacarborane derivatives of 1,1′-bis-(*ortho*-carborane), specifically compounds **1**, **2**α, **2**β, **3**α, and **3**β. All have the rhodacarborane cage present in the 2,1,8-RhC_2B_9 isomeric form, while attached to C8 is, respectively, a $\{1'\text{-}closo\text{-}1',2'\text{-}C_2B_{10}H_{11}\}$ substituent (compound **1**), an $\{8'\text{-}2'\text{-}(p\text{-cymene})\text{-}closo\text{-}2',1',8'\text{-}RuC_2B_9H_{10}\}$ substituent (compounds **2**α and **2**β), or an $\{8'\text{-}2'\text{-}Cp^*\text{-}closo\text{-}2',1',8'\text{-}CoC_2B_9H_{10}\}$ substituent (compounds **3**α and **3**β). All five new compounds have the potential to act as precatalysts since they are $[\{RhH(PPh_3)_2\}(\text{carborane})]$ species similar to Hawthorne's classic compound $[3\text{-}H\text{-}3,3\text{-}(PPh_3)_2\text{-}closo\text{-}3,1,2\text{-}RhC_2B_9H_{11}]$ (**I**) and its 2,1,12-RhC_2B_9 isomer (**V**), and to provide a comparison for the catalytic performances of the new compounds we have resynthesized **I** and **V** and included them in our catalytic studies. The 2,1,12 isomer **V** has previously been characterized by elemental analysis, IR spectroscopy, ^{31}P NMR spectroscopy, and partial ^1H NMR spectroscopy.[11] Here, we report the full ^1H NMR spectrum, the $^{11}B\{^1H\}$ NMR spectrum, and we confirm the structure crystallographically (Figure 9). As was the case with compound **1**, in **V** the $\{RhH(PPh_3)_2\}$ fragment caps a CB_4 carborane ligand face with the hydride ligand lying *trans* to C1, resulting in a long, weak Rh2−C1 connectivity and a low frequency (δ 1.49 ppm) C1*H* chemical shift.

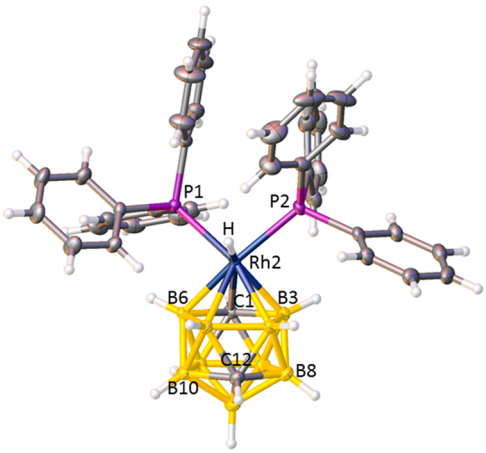

Figure 9. Perspective view of compound **V** with displacement ellipsoids as in Figure 5. Selected interatomic distances (Å): Rh2−C1 2.311(2), Rh2−B3 2.229(2), Rh2−B7 2.214(2), Rh2−B11 2.208(2), Rh2−B6 2.191(2), Rh2−P1 2.3502(5), Rh2−P2 2.3539(5), Rh2−H 1.50(2).

^{103}Rh NMR Study of I and V. For completeness, we have also undertaken a ^{103}Rh NMR investigation of **I** and **V**, specifically to address the question of ^{103}Rh chemical shifts for these types of rhodacarborane clusters. This was possible through access to suitable quantities of the compounds in a form amenable to both direct and indirect ^{103}Rh signal detection. While there has historically been some confusion over the reporting and referencing of ^{103}Rh chemical shifts, the accepted convention now uses a reference value $\Xi(^{103}Rh)$ equal to 3.16 MHz for an NMR spectrometer where the protons of a sample of tetramethylsilane (TMS) resonate at a frequency of exactly 100.0 MHz. Referencing under this condition for a ^{103}Rh chemical shift of 0 ppm for a spectrometer whose TMS 0 ppm proton resonance occurs at 600.130 MHz yields a ^{103}Rh 0 ppm reference frequency equal to 18.964108 MHz. This reference determines that at the magnetic field strength used in this work, 1 ppm for ^{103}Rh is equivalent to 18.964108 Hz. Through this approach, the relative ^{103}Rh chemical shifts for **I** and **V** were obtained. The ^{103}Rh NMR resonance for **I** was found at a frequency of 18.9456572 MHz, equivalent to a chemical shift $\delta^{103}Rh$ = −972.93 ppm. Similarly, the ^{103}Rh resonance for **V** was found at a frequency of 18.9466140 MHz, equivalent to a chemical shift $\delta^{103}Rh$ = −922.48 ppm. The difference, $\Delta\delta^{103}Rh(\mathbf{V} - \mathbf{I})$ = 50.45 ppm with the higher chemical shift occurring for **V**.

^{103}Rh (spin = 1/2) is 100% naturally abundant. However, with a low, negative magnetogyric ratio (-0.845×10^7 rad T^{-1} s^{-1}) and a low resonance frequency (15.737 MHz at a magnetic field strength of 11.74 T) it has an absolute sensitivity compared to proton of 3.11×10^{-5}. These features are compounded by a very wide chemical shift range (10000 ppm $\geq \delta^{103}Rh \geq$ −2000 ppm) and long ^{103}Rh T_1 relaxation times, which ensure that direct observation of ^{103}Rh NMR signals remains challenging. However, provided the NMR spectrometer hardware is suitable for meeting the resonance condition of ^{103}Rh, opportunities, including those reported here, are available to make ^{103}Rh NMR measurements possible. These are largely compound and, specifically, spin-system dependent. To our knowledge there are no previous reports of ^{103}Rh NMR studies of rhodaborane or rhodacarborane clusters, making the present work all the more significant. Indeed, NMR spectroscopic measurements of transition-metal nuclei generally in metallacarboranes are very limited, with rare exceptions including ^{195}Pt, ^{57}Fe, and ^{59}Co.[26]

The preferred approach to detecting ^{103}Rh is indirectly by polarization transfer from a more abundant spin-1/2 nucleus such as ^{1}H or ^{31}P. Precedent demonstrating the benefit of using two-dimensional inverse NMR experiments such as 2D $[^1H, ^{103}Rh]$ HMQC and related NMR methods used to report $\delta^{103}Rh$ began to appear in the literature around the turn of the millennium.[27] The power in comparing experimentally measured $\delta^{103}Rh$ values with those determined theoretically by DFT calculations is also demonstrated in that work.

In this study, the presence in **I** and **V** of the hydride ligand (giving rise to measurable $^1J_{HRh}$ scalar-coupling) provides access to their investigation by ^{103}Rh NMR, which benefits from the boost in sensitivity afforded through polarization transfer between the rhodium nucleus and its directly attached proton. While direct observation of 1D $^{103}Rh\text{-}\{^1H\}$-INEPT provides a sensitivity gain of 31.8 over that of a direct, single-pulse observation approach, a much more sensitive option is via 2D $[^1H, ^{103}Rh]$ HMQC, for which the equivalent sensitivity gain is 5610 times that of direct observation of the ^{103}Rh response. For these pragmatic reasons in this work, $^{103}Rh\text{-}\{^1H\}$-INEPT was used for frequency and pulse calibration purposes using the more abundant sample, and 2D $[^1H, ^{103}Rh]$

https://dx.doi.org/10.1021/acs.inorgchem.9b03351
Inorg. Chem. XXXX, XXX, XXX−XXX

HMQC was subsequently used to refine the accurate identification of ^{103}Rh chemical shifts from both **I** and **V**, owing to the speed with which the data could be repeatedly acquired. The resulting data and full experimental details used to acquire it are provided in the SI, including the methods used to find and confirm the ^{103}Rh resonance frequencies for **I** and **V** and to calibrate ^{103}Rh pulse lengths and transmitter powers. Briefly, the hydride ^{1}H NMR signal for the more abundant **I** was measured under conditions used for indirect heteronuclear pulse calibration (Bruker pulse program decp90). Optimization of the ^{103}Rh 90° pulse length (30 μs at 125.89 W) was followed by a check for signal antialiasing in 2D [^{1}H, ^{103}Rh] HMQC NMR spectra using repeated measurements with variations in ^{103}Rh transmitter frequency offset and the frequency width of the indirectly detected (^{103}Rh) dimension until no further changes in resonance position were observed for signals arising from either **I** or **V**.

It is well established that ^{103}Rh nuclear shielding is very sensitive to small changes in the environment of the rhodium atom,[28] and understanding the relationship requires access to a calibrated series of related compounds, experimental measurement, and computational DFT calculations to unpick the interplay between the various contributing factors to the transition-metal NMR chemical shift. What may be expected in theory is that the formal oxidation state would play the major role in determining chemical shift, but this is not the case in practice.[29] More strongly influencing effects are variations in the type, number, and geometric arrangement of ligands, resulting in changes to the ligand field at the metal center. Consequently, it is clear that a full understanding of how these various factors affect δ^{103}Rh would require access to a complete series of structures related to those reported here, which is beyond the scope of the current article.

Catalysis. The isomerization of terminal alkenes and the hydrosilylation of ketones are two classic reactions catalyzed by a range of transition-metal compounds. As such they represent convenient reactions by which to both assess the potential of new catalyst precursors and compare the effectiveness of these new species against established catalysts. Accordingly, we have tested the abilities of the new rhodacarborane−carborane species **1** and the rhodacarborane−metallacarborane species **2** and **3** against that of the single-cage rhodacarboranes **I** and **V** to catalyze these two reactions. Since the rhodacarboranes cages in **1**, **2**, and **3** are all in the 2,1,8-RhC_2B_9 isomeric form, a more appropriate single-cage comparator than **V** would have been the compound [2-H-2,2-$(PPh_3)_2$-*closo*-2,1,8-$RhC_2B_9H_{11}$] (**XI**), but this is currently unknown. However, we believe that, to a first approximation, **V** serves as an appropriate substitute for **XI** because in both the {$RhH(PPh_3)_2$} fragment is bonded to a CB_4 face of the carborane ligand (Figure 10). Note that

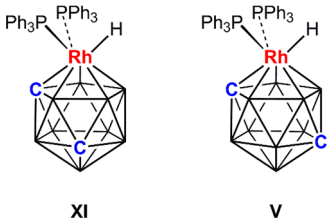

Figure 10. Comparison of [2-H-2,2-$(PPh_3)_2$-*closo*-2,1,8-$RhC_2B_9H_{11}$] (**XI**) and [2-H-2,2-$(PPh_3)_2$-*closo*-2,1,12-$RhC_2B_9H_{11}$] (**V**). In both cases the metal fragment is bonded to a CB_4 carborane ligand face.

the use of **I** and **V** as a catalyst for alkene isomerization[2a,3a] and **I** as a catalyst for hydrosilylation[2a] has already been reported by Hawthorne, and that Balagurova et al. have used **I** and analogs of **I** to extend the scope of catalytic hydrosilylation.[5]

Scheme 4 depicts the isomerization of 1-hexene, and the results are displayed graphically in Figure 11. Here "yield"

Scheme 4. Isomerization of 1-Hexene to a Mixture of *cis*- and *trans*-2-Hexenes and 3-Hexenes

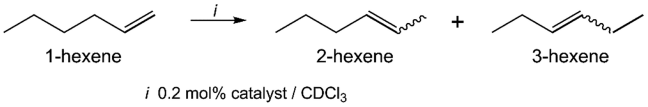

represents the combined yields of *trans*-2-hexene, *cis*-2-hexene, *trans*-3-hexene, and *cis*-3-hexene (a breakdown of these components is given in the SI). In all cases *trans*-2-hexene is the major isomerization product, although significant amounts of the *cis* isomer are also observed. No or very minor amounts of 3-hexenes are formed, consistent with earlier studies.[3a] Compound **I** achieves a yield of ca. 11% after 1 h, ca. 20% after 2 h, and ca. 28% after 3 h. The rhodacarborane−carborane **1** performs better, returning a yield of ca. 41% after 1 h and ca. 65% after 2 h. Better still is the single-cage 2,1,12-RhC_2B_9 species **V**, giving yields of ca. 71% after 1 h and ca. 90% after 2 h. Best of all are the rhodacarborane−metallacarboranes, compounds **2**α, **2**β, **3**α, and **3**β, each achieving yields of >95% after only 1 h.

The hydrosilylation of acetophenone by diphenylsilane is shown in Scheme 5, resulting in a mixture of the silyl ether diphenyl(1-phenylethoxy)silane and the silyl enol ether diphenyl{(1-phenylvinyl)oxy}silane. The results of the use of **I**, **V**, **1**, **2**α, **2**β, **3**α, and **3**β to catalyze this reaction are displayed as Figure 12 (again "yield" refers to the combined yield of the two products, with a breakdown available in the SI). Compared to alkene isomerization this reaction is generally more sluggish, requiring heating to 55 °C and longer reaction times to achieve significant yields. Now the two single-cage species, **I** and **V**, perform best, achieving yields of ca. 89% and 99% after 2 h. Next comes the rhodacarborane−carborane compound **1**, returning a yield of ca. 43% after 2 h, while the slowest reactions are those catalyzed by rhodacarborane−metallacarborane species **2**α, **2**β, **3**α, and **3**β, affording yields of only ca. 20−31% in the same time.

How can these experimental results be rationalized in mechanistic terms? In the case of hydrosilylation the single-cage rhodacarboranes (**V** and **I**) are the best, while those with a carborane substituent (**1**) and a metallacarborane substituent (**2**, **3**) are progressively poorer. This strongly suggests that the additional steric bulk of the bis(carborane) derivatives is responsible for their diminished catalytic activity. It is generally accepted that the most reasonable mechanism for rhodium-catalyzed hydrosilylation of ketones with dihydrosilanes is the Hofmann−Gade mechanism[30] which is subsequently extended by Kühn et al. to account for the coformation of silyl enol ether.[31] In both cases a key step is oxidative addition of Si−H to a coordinatively unsaturated Rh^{I} center, presumably similar in form to the *exonido* species **II** (Figure 2).

In the isomerization of 1-hexene the pattern is almost reversed, in that single-cage **I** is now the worst catalyst, then the rhodacarborane−carborane **1**, and then the rhodacarborane−metallacarboranes **2** and **3** performing best. However,

https://dx.doi.org/10.1021/acs.inorgchem.9b03351
Inorg. Chem. XXXX, XXX, XXX−XXX

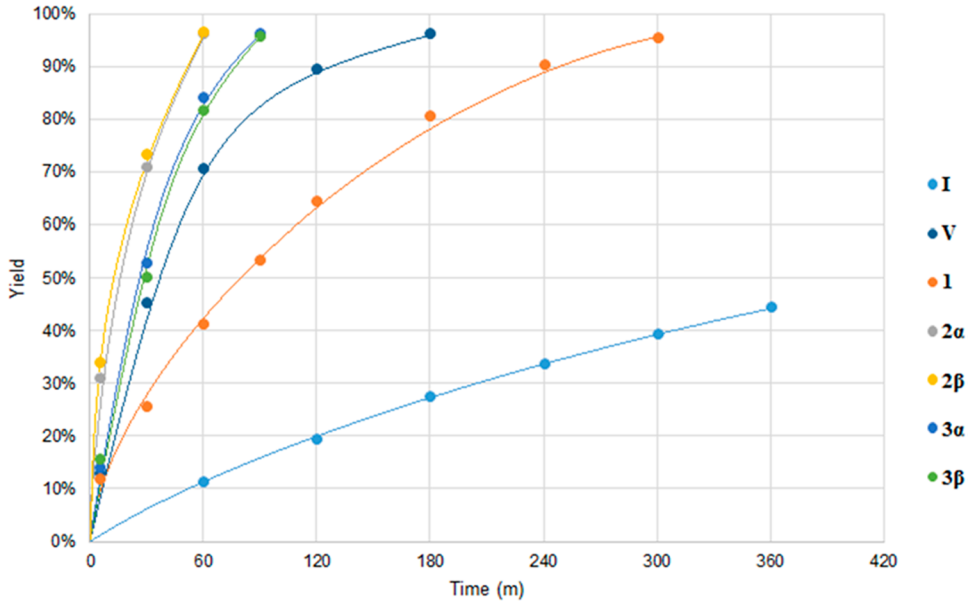

Figure 11. Catalytic results for the isomerization of 1-hexene.

Scheme 5. Hydrosilylation of Acetophenone by Diphenylsilane to Afford a Mixture of Silyl Ether and Silyl Enol Ether

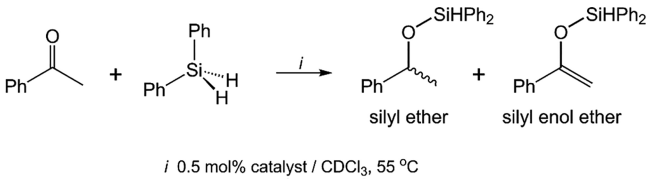

single-cage **V** is also very effective, as a better catalyst than **1** and nearly as good as **2** and **3**. In broad terms, if increased steric crowding could be used to rationalize the relative catalytic performance of the rhodacarboranes in hydrosilylation, that is not the case for alkene isomerization.

It is particularly challenging to understand the relative catalytic performance of **I** and **V** with respect to alkene isomerization. As noted in the Introduction, from kinetic and deuterium labeling studies, it was concluded that the active catalyst for alkene isomerization by rhodacarborane **I** was the product of phosphine loss from the Rh^{III} hydride **III**, a derivative of the *exonido* tautomer **II** formed from **I** by reductive decoupling of the $\{Rh(PPh_3)_2\}$ fragment from the carborane ligand face. In a metallacarborane the M−B connectivities are generally stronger than the M−C connectivities (because the frontier molecular orbitals of a carborane ligand are predominantly localized on the B atoms[32]) meaning that, everything else being equal, a carborane with a CB_4 ligand face would be bound more strongly to a metal atom than one with a C_2B_3 ligand face. Consequently, it would be reasonable to suggest that the

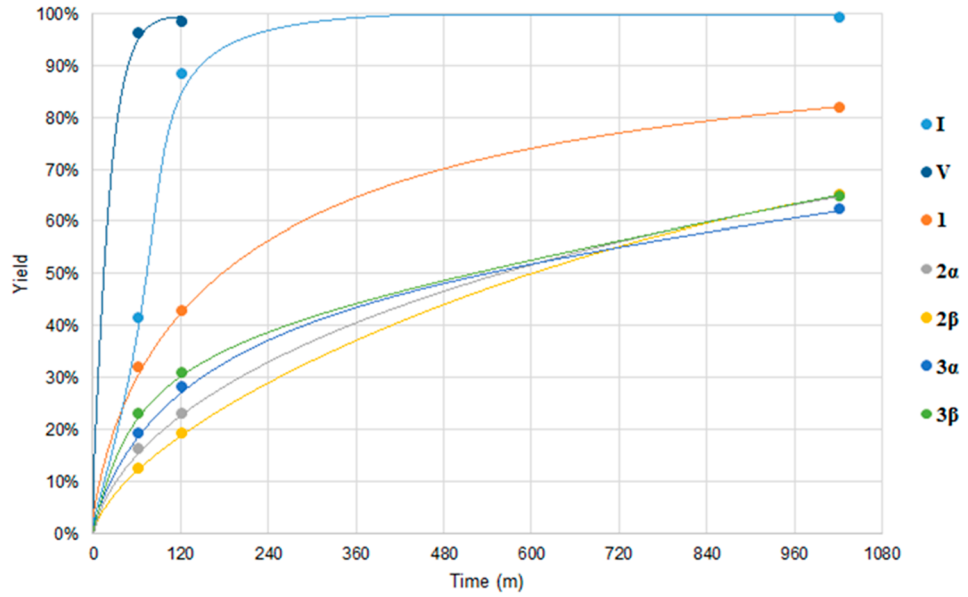

Figure 12. Catalytic results for the hydrosilylation of acetophenone by diphenylsilane.

https://dx.doi.org/10.1021/acs.inorgchem.9b03351
Inorg. Chem. XXXX, XXX, XXX−XXX

activation barrier for the *closo*-to-*exonido* tautomerism outlined in Figure 2 would be significantly higher for **V** (and by extension **1**, **2**, and **3**) than that for **I**, yet **I** is the worst catalyst.

This leads to the tempting suggestion that it is possible that the 3,1,2-RhC_2B_9 species **I** and the 2,1,8- or 2,1,12-RhC_2B_9 species **1**−**3** and **V** operate in alkene isomerization by differing mechanisms. The detailed mechanistic studies on **I** date from the 1980s, since which time further investigations into the use of rhodacarboranes as homogeneous catalyst precursors have been sparce. During this period, however, the development of density functional theory (DFT) and its application in elucidating complex reaction mechanisms has become an exceptionally powerful and important part of modern-day chemistry.[33] It therefore seems appropriate to suggest that a thorough DFT investigation of the mechanism of reactions catalyzed by metallacarboranes, particularly rhodacarboranes, is overdue. We hope that the experimental results described herein will stimulate such a study, which would complement recent research into the use of *closo*-carborane anions in catalysis.[34]

■ CONCLUSIONS

The rhodacarborane **1**, a derivative of 1,1′-bis(*ortho*-carborane), and related rhodacarborane−ruthenacarborane (**2**) and rhodacarborane−cobaltacarborane (**3**) compounds have been prepared and characterized, and the known single-cage compounds **I** and **V** have been the subject of the first ^{103}Rh NMR studies of rhodacarboranes. In catalyzing the hydrosilylation of acetophenone, the single-cage species **I** and **V** perform better than the double-cage compounds **1**, **2**, and **3**, potentially a consequence of greater steric crowding in **1**−**3** that restricts the oxidative addition of Si−H to the metal center. In catalyzing the isomerization of 1-hexene the 3,1,2-RhC_2B_9 species **I** performs significantly worse than the 2,1,8- or 2,1,12-RhC_2B_9 species **V**, **1**, **2**, and **3**, which may suggest that the mechanism of alkene isomerization catalyzed by rhodacarboranes depends upon the isomeric form of the catalyst.

■ ASSOCIATED CONTENT

Supporting Information

The Supporting Information is available free of charge at https://pubs.acs.org/doi/10.1021/acs.inorgchem.9b03351.

This information comprises NMR spectra of all new products, details of the ^{103}Rh NMR study of **I** and **V**, and details of the catalytic experiments (PDF)

Accession Codes

CCDC 1964963−1964968 contain the supplementary crystallographic data for this paper. These data can be obtained free of charge via www.ccdc.cam.ac.uk/data_request/cif, or by emailing data_request@ccdc.cam.ac.uk, or by contacting The Cambridge Crystallographic Data Centre, 12 Union Road, Cambridge CB2 1EZ, UK; fax: +44 1223 336033.

■ AUTHOR INFORMATION

Corresponding Author

Alan J. Welch − *Heriot-Watt University, Edinburgh, United Kingdom;* orcid.org/0000-0003-4236-2475; Email: a.j.welch@hw.ac.uk

Other Authors

Antony P.Y. Chan − *Heriot-Watt University, Edinburgh, United Kingdom*

John A. Parkinson − *University of Strathclyde, Glasgow, United Kingdom;* orcid.org/0000-0003-4270-6135

Georgina M. Rosair − *Heriot-Watt University, Edinburgh, United Kingdom;* orcid.org/0000-0002-4079-0938

Complete contact information is available at: https://pubs.acs.org/10.1021/acs.inorgchem.9b03351

Notes

The authors declare no competing financial interest.

■ ACKNOWLEDGMENTS

We thank the Engineering and Physical Sciences Research Council and the CRITICAT Centre for Doctoral Training for financial support (Ph.D. studentship to A.P.Y.C.; EP/L016419/1). We also thank the U.K. National Crystallography Service for data collection of compounds **1**·0.5CH_2Cl_2, **2**α·2CH_2Cl_2, and **2**β·1.5CH_2Cl_2 and Dr. C. Wilson (Univ. of Glasgow) for data collection of compound **V**.

■ REFERENCES

(1) Grimes, R. N. Chapter 15. *Carboranes*, 3 rd ed.; Elsevier: Amsterdam, The Netherlands, 2016; pp 929−944.

(2) (a) Paxson, T. E.; Hawthorne, M. F. Preparation of hydridometallocarboranes and their use as homogeneous catalysts. *J. Am. Chem. Soc.* **1974**, *96*, 4674−4676. (b) Baker, R. T.; Delaney, M. S.; King, R. E., III; Knobler, C. B.; Long, J. A.; Marder, T. B.; Paxson, T. E.; Teller, R. G.; Hawthorne, M. F. Metallacarboranes in Catalysis. 2. Synthesis and Reactivity of Closo Icosahedral Bis(phosphine)-hydridorhodacarboranes and the Crystal and Molecular Structures of Two Unusual *closo*-Phosphinerhodacarborane Complexes. *J. Am. Chem. Soc.* **1984**, *106*, 2965−2978.

(3) (a) Behnken, P. E.; Belmont, J. A.; Busby, D. C.; Delaney, M. S.; King, R. E., III; Kreimendahl, C. W.; Marder, T. B.; Wilczynski, J. J.; Hawthorne, M. F. Metallacarboranes in Catalysis. 6. Kinetics and Mechanism of Alkene Hydrogenation and Isomerization Catalyzed by Rhodacarborane Clusters. A Search for Cluster Catalysis. *J. Am. Chem. Soc.* **1984**, *106*, 3011−3025. (b) Belmont, J. A.; Soto, J.; King, R. E., III; Donaldson, A. J.; Hewes, J. D.; Hawthorne, M. F. Metallacarboranes in Catalysis. 8. I: Catalytic Hydrogenolysis of Alkenyl Acetates. II. Catalytic Alkene Isomerization and Hydrogenation Revisited. *J. Am. Chem. Soc.* **1989**, *111*, 7475−7486.

(4) (a) Long, J. A.; Marder, T. B.; Behnken, P. E.; Hawthorne, M. F. Metallacarboranes in Catalysis. 3. Synthesis and Reactivity of *exo-nido*-Phosphinerhodacarboranes. *J. Am. Chem. Soc.* **1984**, *106*, 2979−2989. (b) Knobler, C. B.; Marder, T. B.; Mizusawa, E. A.; Teller, R. G.; Long, J. A.; Behnken, P. E.; Hawthorne, M. F. Metallacarboranes in Catalysis. 4. Structures of *closo*- and *exo-nido*-Phosphinerhodacarboranes and a $[(PPh_3)_3Rh]^+[nido\text{-}7\text{-}R\text{-}7,8\text{-}C_2B_9H_{11}]^-$ Salt. *J. Am. Chem. Soc.* **1984**, *106*, 2990−3004.

(5) Lebedev, V. N.; Balagurova, E. V.; Dolgushin, F. M.; Yanovskii, A. I.; Zakharkin, L. I. Fluorosubstituted rhodacarboranes 3,3-$(R_3P)_2$-3-H-3,1,2-$RhC_2B_9H_{11-n}F_n$ (n = 1, 2, 4): synthesis, molecular structure, and catalytic properties in hydrosilylation of styrene and phenylacetylene. *Russ. Chem. Bull.* **1997**, *46*, 550−558.

(6) Allcock, H. R.; Scopelianos, A. G.; Whittle, R. R.; Tollefson, N. M. Cyclic and High Polymeric *nido*-Carboranylphosphazenes as Ligands for Transition Metals. *J. Am. Chem. Soc.* **1983**, *105*, 1316−1321.

(7) Recent publications (a) Sivaev, I. B.; Bregadze, V. I. 1,1′-Bis(*ortho*-carborane)-based transition metal complexes. *Coord. Chem. Rev.* **2019**, *392*, 146−176 and references therein.. (b) Yruegas, S.;

Axtell, J. C.; Kirlikovali, K. O.; Spokoyny, A. M.; Martin, C. D. Synthesis of 9-borafluorene analogues featuring a three-dimensional 1,1′-bis(*o*-carborane) backbone. *Chem. Commun.* **2019**, *55*, 2892−2895. (c) Wu, J.; Cao, K.; Zhang, C.-Y.; Xu, T.-T.; Ding, L.-F.; Li, B.; Yang, J. Catalytic Oxidative Dehydrogenative Coupling of Cage B-H/B-H Bonds for Synthesis of Bis(*o*-carborane)s. *Org. Lett.* **2019**, *21*, 5986−5989. (d) Jeans, R. J.; Chan, A. P. Y.; Riley, L. E.; Taylor, J.; Rosair, G. M.; Welch, A. J.; Sivaev, I. B. Arene-Ruthenium Complexes of 1,1′-Bis(*ortho*-carborane): Synthesis, Characterization, and Catalysis. *Inorg. Chem.* **2019**, *58*, 11751−11761. (e) Benton, A.; Durand, D. J.; Copeland, Z.; Watson, J. D.; Fey, N.; Mansell, S. M.; Rosair, G. M.; Welch, A. J. On the Basicity of Carboranylphosphines. *Inorg. Chem.* **2019**, *58*, 14818−14829.

(8) (a) Thiripuranathar, G.; Man, W. Y.; Palmero, C.; Chan, A. P. Y.; Leube, B. T.; Ellis, D.; McKay, D.; Macgregor, S. A.; Jourdan, L.; Rosair, G. M.; Welch, A. J. Icosahedral metallacarborane/carborane species derived from 1,1′-bis(*o*-carborane). *Dalton Trans.* **2015**, *44*, 5628−5637. (b) Mandal, D.; Man, W. Y.; Rosair, G. M.; Welch, A. J. Steric*versus* electronic factors in metallacarborane isomerisation: nickelacarboranes with 3,1,2-, 4,1,2- and 2,1,8-NiC_2B_9 architectures and pendant carborane groups, derived from 1,1′-bis(*o*-carborane). *Dalton Trans.* **2016**, *45*, 15013−15025.

(9) Thiripuranathar, G.; Chan, A. P. Y.; Mandal, D.; Man, W. Y.; Argentari, M.; Rosair, G. M.; Welch, A. J. Double deboronation and homometalation of 1,1′-bis(*ortho*-carborane). *Dalton Trans.* **2017**, *46*, 1811−1821.

(10) Chan, A. P. Y.; Rosair, G. M.; Welch, A. J. Heterometalation of 1,1′-bis(*ortho*-carborane). *Inorg. Chem.* **2018**, *57*, 8002−8011.

(11) Busby, D. C.; Hawthorne, M. F. The Crown Ether Promoted Base Degradation of *p*-Carborane. *Inorg. Chem.* **1982**, *21*, 4101−4103.

(12) Ren, S.; Xie, Z. A Facile and Practical Synthetic Route to 1,1′-Bis(*o*-carborane). *Organometallics* **2008**, *27*, 5167−5168 Note that the ^{1}H NMR chemical shift (δ = 5.51 ppm) reported in this paper for the C2*H* and C2′*H* atoms of 1,1′-bis(*ortho*-carborane) in $(CD_3)_2CO$ is at variance with the value (δ = 5.05 ppm) that we and others record (e.g.. Yang, X.; Jiang, W.; Knobler, C. B.; Mortimer, M. D.; Hawthorne, M. F. The synthesis and structural characterization of carborane oligomers connected by carbon-carbon and carbon-boron bonds between icosahedra. *Inorg. Chim. Acta* **1995**, *240*, 371−378.

(13) Osborn, J. A.; Wilkinson, G.; Mrowca, J. J. Chlorotris-(triphenylphosphine)rhodium(I) (Wilkinson's catalyst). *Inorg. Synth.* **2007**, *28*, 77−79.

(14) Note that in these descriptions of **VIII** and **IX** the primed and unprimed cages have been swapped to allow the rhodacarborane cages in the products **2** and **3** to be unprimed, consistent with that in **1**. Thus, anion **VIII** should formally be [8-(7′-*nido*-7′,8′-$C_2B_9H_{11}$)-2-(*p*-cymene)-*closo*-2,1,8-$RuC_2B_9H_{10}$]$^{-10}$ but is referred to here as [8′-(7-*nido*-7,8-$C_2B_9H_{11}$)-2′-(*p*-cymene)-*closo*-2′,1′,8′-$RuC_2B_9H_{10}$]$^-$, and anion **IX** should formally be [8-(7′-*nido*-7′,8′-$C_2B_9H_{11}$)-2-Cp*-*closo*-2,1,8-$CoC_2B_9H_{10}$]$^{-10}$ but is referred to here as [8′-(7-*nido*-7,8-$C_2B_9H_{11}$)-2′-Cp*-*closo*-2′,1′,8′-$CoC_2B_9H_{10}$]$^-$.

(15) Dolomanov, O. V.; Bourhis, L. J.; Gildea, R. J.; Howard, J. A. K.; Puschmann, H. *OLEX2*: a complete structure solution, refinement and analysis program. *J. Appl. Crystallogr.* **2009**, *42*, 339−341.

(16) Sheldrick, G. M. A short history of *SHELX*. *Acta Crystallogr., Sect. A: Found. Crystallogr.* **2008**, *64*, 112−122.

(17) Sheldrick, G. M. *SHELXT* − Integrated space-group and crystal-structure determination. *Acta Crystallogr., Sect. A: Found. Crystallogr.* **2015**, *71*, 3−8.

(18) Sheldrick, G. M. Crystal structure refinement with *SHELXL*. *Acta Crystallogr., Sect. C: Struct. Chem.* **2015**, *71*, 3−8.

(19) van der Sluis, P.; Spek, A. L. *BYPASS*: an effective method for the refinement of crystal structures containing disordered solvent regions. *Acta Crystallogr., Sect. A: Found. Crystallogr.* **1990**, *46*, 194−201.

(20) (a) McAnaw, A.; Scott, G.; Elrick, L.; Rosair, G. M.; Welch, A. J. The VCD method − a simple and reliable way to distinguish cage C and B atoms in (hetero)carborane structures determined crystallographically. *Dalton Trans.* **2013**, *42*, 645−664. (b) McAnaw, A.; Lopez, M. E.; Ellis, D.; Rosair, G. M.; Welch, A. J. Asymmetric 1,8/13,2,*x*-$M_2C_2B_{10}$ 14-vertex metallacarboranes by direct electrophilic insertion reactions; the VCD and BHD methods in critical analysis of cage C atom positions. *Dalton Trans.* **2014**, *43*, 5095−5105. (c) Welch, A. J. What Can We Learn from the Crystal Structures of Metallacarboranes? *Crystals* **2017**, *7*, 234.

(21) Lopez, M. E.; Edie, M. J.; Ellis, D.; Horneber, A.; Macgregor, S. A.; Rosair, G. M.; Welch, A. J. Symmetric and asymmetric 13-vertex bimetallacarboranes by polyhedral expansion. *Chem. Commun.* **2007**, 2243−2245.

(22) (a) Burke, A.; McIntosh, R.; Ellis, D.; Rosair, G. M.; Welch, A. J. 13-Vertex carbacobaltaboranes: synthesis and molecular structures of the 4,1,6-, 4,1,8- and 4,1,12-isomers of Cp*$CoC_2B_{10}H_{12}$. *Collect. Czech. Chem. Commun.* **2002**, *67*, 991−1006. (b) Burke, A. Supraicosahedral metallacarboranes. Ph.D. Thesis, Heriot-Watt University, U.K., 2004.

(23) (a) Ferguson, G.; McEneaney, P. A.; Spalding, T. R. 3-Chloro-3,3-bis(triphenylphosphine-*P*)1,2-dicarba-3-rhoda-*closo*-dodecaborane-Dichloromethane (1/1.1). *Acta Crystallogr., Sect. C: Cryst. Struct. Commun.* **1996**, *52*, 2710−2713. (b) Chizhevsky, I. T.; Pisareva, I. V.; Vorontzov, E. V.; Bregadze, V. I.; Dolgushin, F. M.; Yanovsky, A. I.; Struchkov, Yu. T.; Knobler, C. B.; Hawthorne, M. F. Synthesis, structure and reactivity of a novel monocarbonhydridorhodacarborane*closo*-2,2-$(Ph_3P)_2$-2-H-1-(Me_3N)-2,1-$RhCB_{10}H_{10}$ molecular structure of 16-electron *closo*-2-(Ph_3P)-2-Cl-1-(Me_3N)-2,1-$RhCB_{10}H_{10}$ and closely related 18-electron *closo*-3,3-$(Ph_3P)_2$-3-Cl-3,1,2-$RhC_2B_9H_{11}$. *J. Organomet. Chem.* **1997**, *536*−*537*, 223−231.

(24) Chizhevsky, I. T.; Lobanova, I. A.; Petrovskii, P. V.; Bregadze, V. I.; Dolgushin, F. M.; Yanovsky, A. I.; Struchkov, Yu. T.; Chistyakov, A. L.; Stankevich, I. V.; Knobler, C. B.; Hawthorne, M. F. Synthesis of Mixed-Metal (Ru-Rh) Bimetallacarboranes via *exo-nido-* and *closo*-Ruthenacarboranes. Molecular Structures of (η^4-C_8H_{12})Rh(μ-H)Ru$(PPh_3)_2$(η^5-$C_2B_9H_{11}$) and (CO)(PPh_3)Rh(μ-H)-Ru$(PPh_3)_2$(η^5-$C_2B_9H_{11}$) and Their Anionic *closo*-Ruthenacarborane Precursors. *Organometallics* **1999**, *18*, 726−735.

(25) Doi, J. A.; Mizusawa, E. A.; Knobler, C. B.; Hawthorne, M. F. Rearrangement of *closo*-3,3-$(PPh_3)_2$-3-H-1-(R)-3,1,2-$IrC_2B_9H_{10}$ to *closo*-2,2-$(PPh_3)_2$-3-H-8-(R)-2,1,8-$IrC_2B_9H_{10}$. Synthesis and X-ray Structure of *closo*-2,2-$(PPh_3)_2$-2-H-8-(C_6H_5)-2,1,8-$IrC_2B_9H_{10}$. *Inorg. Chem.* **1984**, *23*, 1482−1484.

(26) (a) Green, M.; Spencer, J. L.; Stone, F. G. A. MetallaboraneChemistry. Part 9. Oxidative-insertion Reactions of Zerovalent Nickel and Platinum Complexes with 1,7-Dicarba-*closo*-octaborane, 4,5-Dicarba-*closo*-nonaborane, 1,6-Dicarba-*closo*-decaborane, and their *C*-Methyl Derivatives. *J. Chem. Soc., Dalton Trans.* **1979**, 1679−1686. (b) Wrackmeyer, B.; Schanz, H.-J. Hexaethyl-2,4-dicarba-*nido*-hexaborane(8), Deprotonation and Complexation Studied by NMR Spectroscopy and Density Functional Theory (DFT) Calculations. *Z. Naturforsch., B: J. Chem. Sci.* **2004**, *B59*, 685−691. (c) Ooms, K. J.; Terskikh, V. V.; Wasylishen, R. E. Ultrahigh-Field Solid-State ^{59}Co NMR Studies of $Co(C_2B_9H_{11})_2^-$ and $Co(C_5H_5)_2^+$ Salts. *J. Am. Chem. Soc.* **2007**, *129*, 6704−6705.

(27) Orian, L.; Bisello, A.; Santi, S.; Ceccon, A.; Saielli, G. ^{103}Rh NMR Chemical Shifts in Organometallic Complexes: A Combined Experimental and Density Functional Study. *Chem. - Eur. J.* **2004**, *10*, 4029−4040.

(28) (a) Mann, B.; Pregosin, P. S. *Transition Metal Nuclear Magnetic Resonance*; Pregosin, P. S., Ed.; Elsevier: Amsterdam, The Netherlands, 1991; pp 143−215. (b) von Philipsborn, W. Probing organometallic structure and reactivity by transition metal NMR spectroscopy. *Chem. Soc. Rev.* **1999**, *28*, 95−105. (c) Herberhold, M.; Daniel, T.; Daschner, D.; Milius, W.; Wrackmeyer, B. Mononuclear half-sandwich rhodium complexes containing phenylchalcogenolato ligands: a multinuclear (^{1}H, ^{13}C, ^{31}P, ^{77}Se, ^{103}Rh, ^{125}Te) magnetic resonance study. *J. Organomet. Chem.* **1999**, *585*, 234−240.

(29) Ernsting, J. M.; Gaemers, S.; Elsevier, C. J. ^{103}Rh NMR spectroscopy and its application to rhodium chemistry. *Magn. Reson. Chem.* **2004**, *42*, 721−736.

https://dx.doi.org/10.1021/acs.inorgchem.9b03351
Inorg. Chem. XXXX, XXX, XXX−XXX

(30) Schneider, N.; Finger, M.; Haferkemper, C.; Bellemin-Laponnaz, S.; Hofmann, P.; Gade, L. H. Metal Silylenes Generated by Double Silicon-Hydrogen Activation: Key Intermediates in the Rhodium-Catalyzed Hydrosilylation of Ketones. *Angew. Chem., Int. Ed.* **2009**, *48*, 1609−1613.

(31) Riener, K.; Hogerl, M. P.; Gigler, P.; Kuhn, F. E. Rhodium-Catalyzed Hydrosilylation of Ketones: Catalyst Development and Mechanistic Insights. *ACS Catal.* **2012**, *2*, 613−621.

(32) Mingos, D. M. P.; Forsyth, M. I.; Welch, A. J. Molecular and Crystal Structure of 3,3-Bis(triethylphosphine)-1,2-dicarba-3-platina-dodecaborane and Molecular-orbital Analysis of the "Slip" Distortion in Carbametallaboranes. *J. Chem. Soc., Dalton Trans.* **1978**, 1363−1374.

(33) (a) Sperger, T.; Sanhueza, I. A.; Kalvet, I.; Schoenebeck, F. Computational Studies of Synthetically Relevant Homogeneous Organometallic Catalysis Involving Ni, Pd, Ir, and Rh: An Overview of Commonly Employed DFT Methods and Mechanistic Insights. *Chem. Rev.* **2015**, *115*, 9532−9586 and references therein.. (b) Balcells, D.; Clot, E.; Eisenstein, O.; Nova, A.; Perrin, L. Deciphering Selectivity in Organic Reactions: A Multifaceted Problem. *Acc. Chem. Res.* **2016**, *49*, 1070−1078 and references therein.. (c) Davies, D. L.; Macgregor, S. A.; McMullin, C. L. Computational Studies of Carboxylate-Assisted C-H Activation and Functionalization at Group 8−10 Transition Metal Centers. *Chem. Rev.* **2017**, *117*, 8649−8709 and references therein..

(34) Fisher, S. P.; Tomich, A. W.; Lovera, S. O.; Kleinsasser, J. F.; Guo, J.; Asay, M. J.; Nelson, H. M.; Lavallo, V. Nonclassical Applications of *closo*-Carborane Anions: From Main Group Chemistry and Catalysis to Energy Storage. *Chem. Rev.* **2019**, *119*, 8262−8290.

https://dx.doi.org/10.1021/acs.inorgchem.9b03351
Inorg. Chem. XXXX, XXX, XXX−XXX